Study on Waveguide-Type Optical Circuits for Recognition of Optical 8QAM Coded Labels

Doctoral Degree Thesis

TUMENDEMBEREL SURENKHOROL

Tokushima University
Graduate School of Advanced Science and Technology

March 2021

Contents

Chapter 1

Introduction

1.1 Research Background

An advent of optical transmission technologies such as Wavelength Division Multiplexing (WDM) enables today's high speed Internet. However, the usage of broadband services is increasing rapidly year by year due to the the application of advanced technologies like cloud based services, Internet of things (IoT), high definition (HD) video distribution and so on. Figure 1.1 shows a summarized Internet traffic of Japan compiled by Japanese Ministry of Internal Affairs and Communications.

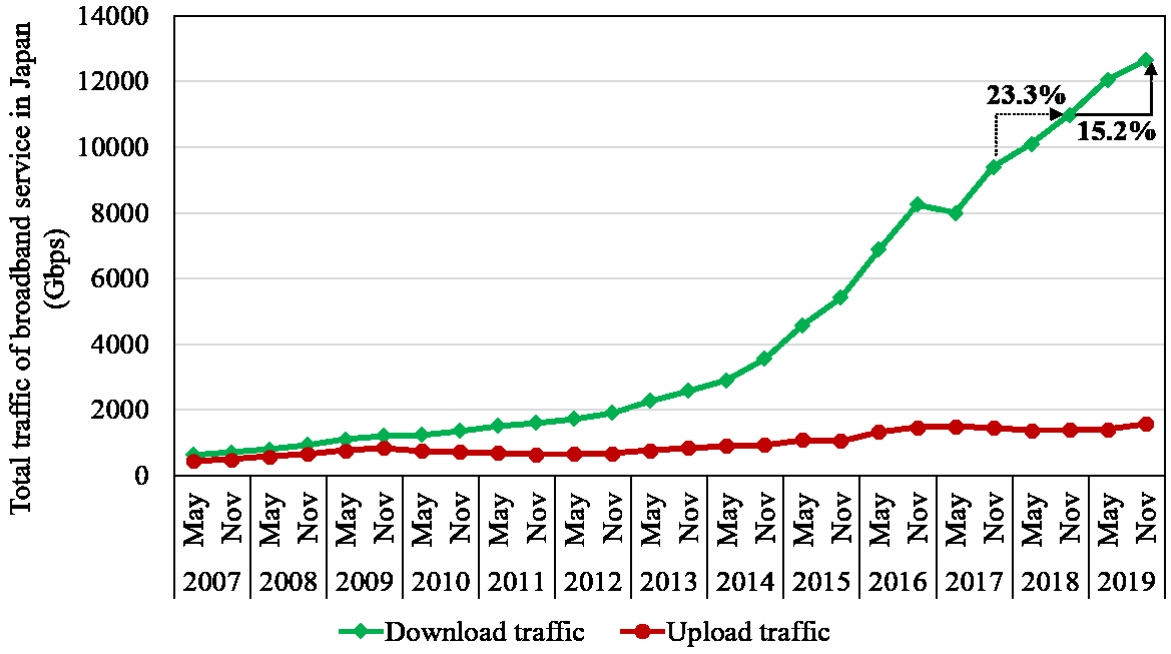

Figure 1.1: Internet traffic statistics of Japan

If traffic growth continues at such pace, current transmission technologies and processing speed of switching nodes won't be able to provide required bandwidth demand. To find a solution for this problem, many factors in communication network are re-discussed and researched for further development.

Simply, communication network consists of connected nodes and links to enable information transfer between users as shown in Figure 1.2.

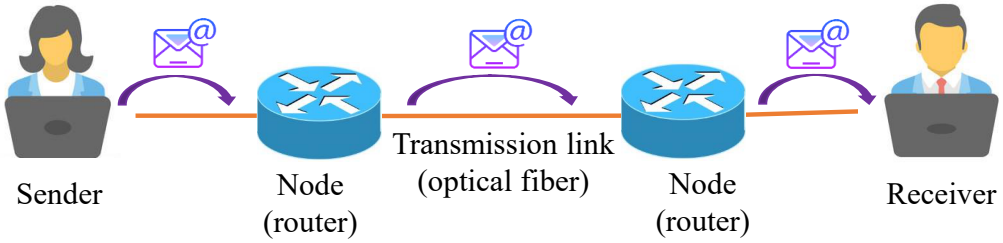

Figure 1.2: Simple structure of communication network

A big obstacle in current network is that signal representing user data is converted from optical to electrical and converted back to optical (OEO) form while it is processed in network nodes. Such conversion between different signal forms causes delay in network and limits network throughput even if the link has enough capacity. To solve this bottleneck issue, as shown in Figure 1.3 (b), optical signal processing needs to be applied in nodes [1].

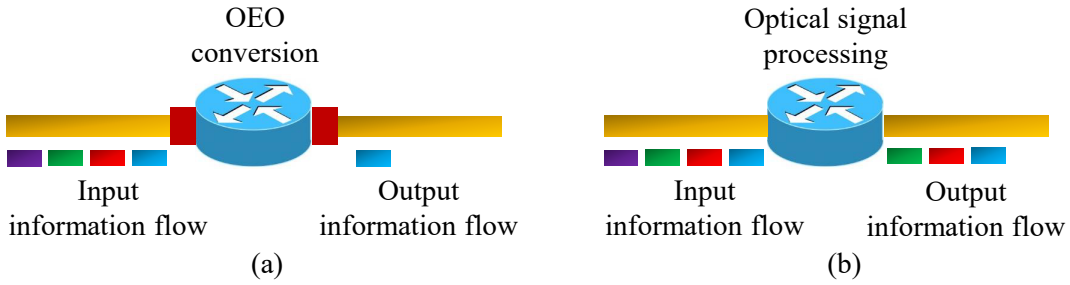

Figure 1.3: Processing speed bottleneck in network node (a) Influence of OEO conversion, (b)Influence of All Optical signal processing

1.1.1 Label Switching Network

In internet network, information such as an email, message, videos is divided into several pieces called packet and an address of destination or next receiving node is attached into each of the packet. A router is main transmission node and its responsibility is to process address, which is called Internet Protocol (IP) address, of the information packet for routing purpose. A label switching is a technique, which is broadly used recently to simplify traditional IP address switching operation. The IP switching method processes long length IP address information of the packet as a forwarding process as shown in Figure 1.4 (a). On the contrary, as depicted in Figure 1.4 (b), label switching method uses shorter labels for routing and it results faster processing speed. It has been studied that most of the Internet traffic flows into several popular destinations such as Youtube, Netflix, Facebook and so on. Therefore, by applying shorter label address into these most used and well known destinations instead of IP address, it can improve transmission and processing speed. Due to this merit, label switching is attractive technique in backbone network. So far, different techniques called Multi Protocol Label Switching (MPLS) and Generalized Multiprotocol Label Switching

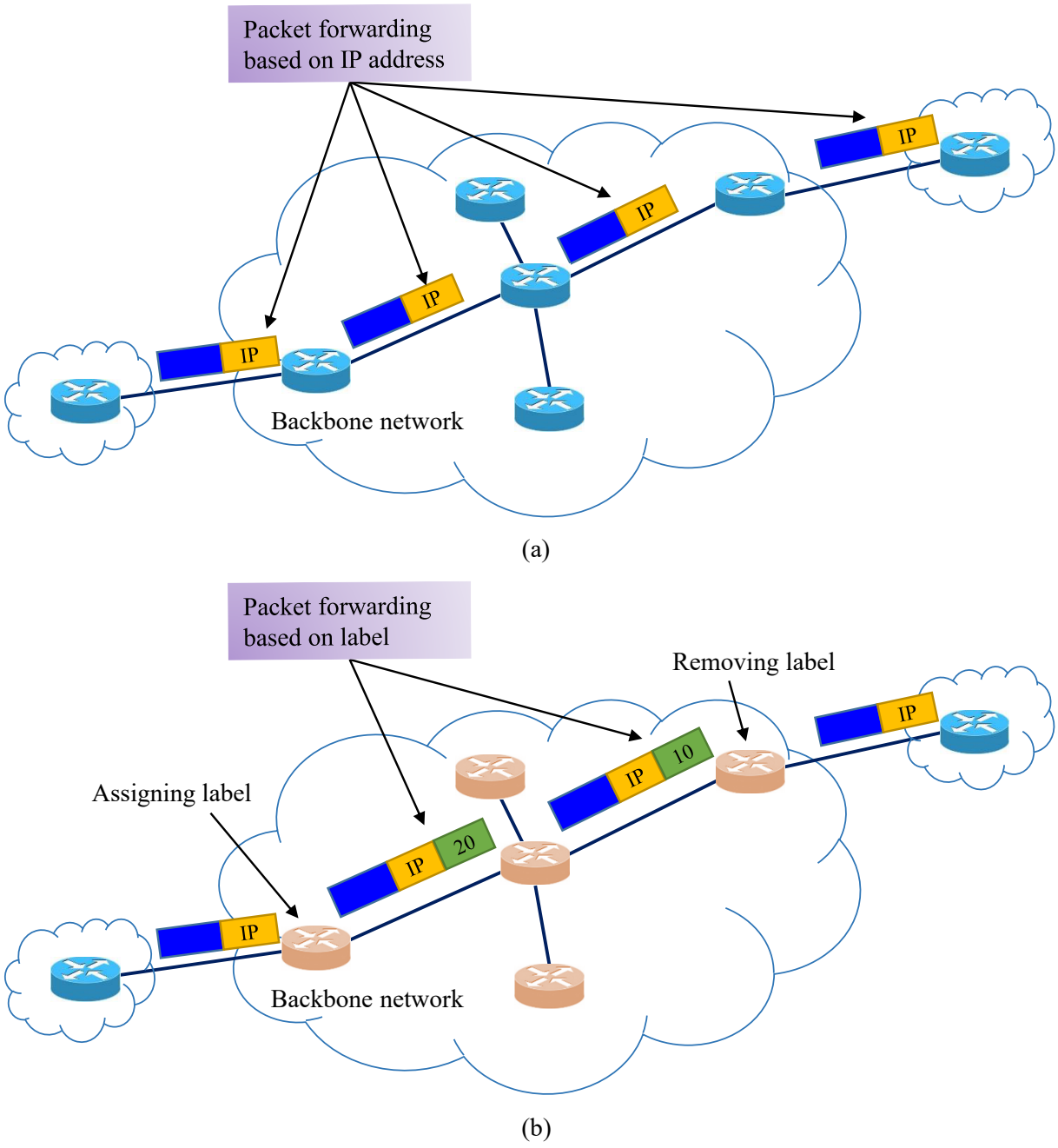

Figure 1.4: Packet switching network ((a) Packet forwarding based on IP address, (b) Packet forwarding based on label)

(GMPLS) have been applied already. Furthermore, All Optical Label Switching (AOLS) [2], which uses optically coded labels and perform switching in only optical domain without electrical processes in photonic label router, is expected to be applied. For such purpose, AOLS has been researched actively.

1.1.2 Optical Code Types

To carry information through communication systems, properties of carrier signal such as frequency, phase or amplitude is varied or modulated [3]. Depending on which of the property is modified, the signal is called on-off-keying (OOK), binary phase shift keying (BPSK), quadrature phase shift keying (QPSK) and quadrature amplitude modulation (QAM). A constellation diagram is used to illustrate the representation of modulated signal in two-dimensional complex plane. The real and imaginary axes of the plane is called the in phase (I) and quadrature (Q), respectively. Each point, named constellation points, on the constellation diagram represents one symbol which is the one or several encoded bits conveying information signal.

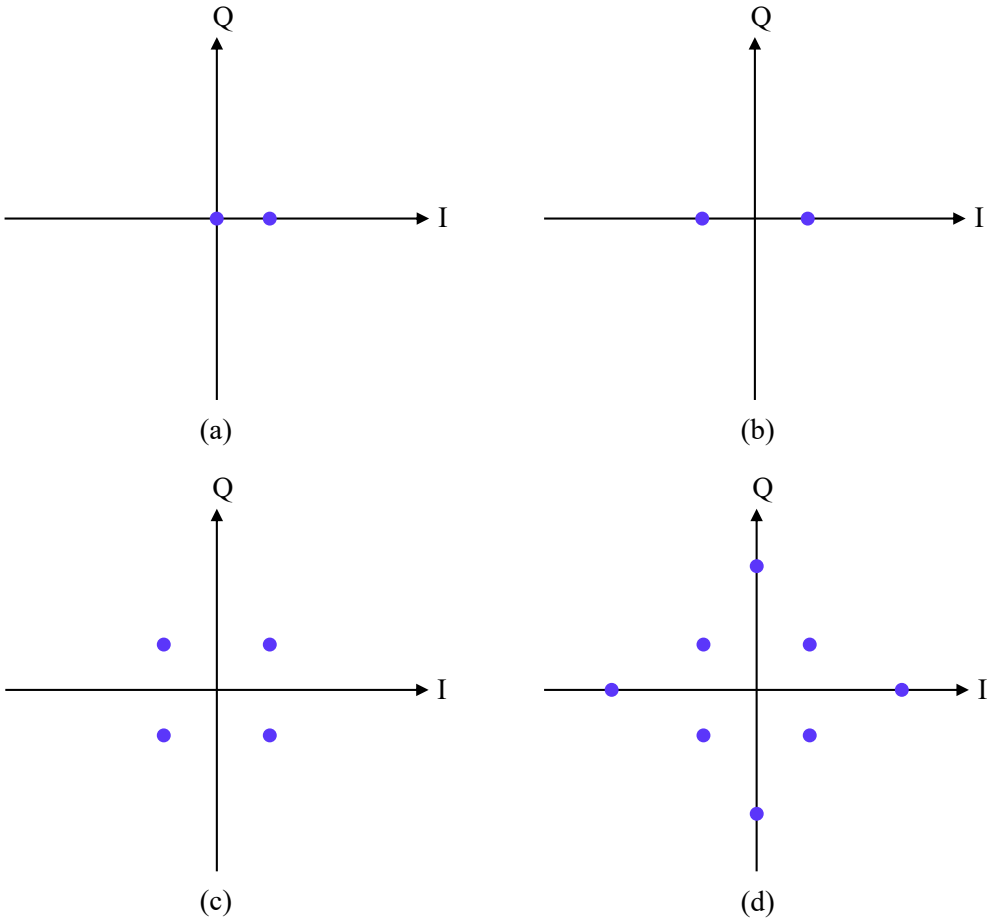

Figure 1.5: Constellation of different code types ((a) OOK, (b) BPSK, (c) QPSK, and (d) 8QAM)

Figure 1.5 shows a constellation diagrams of some modulation formats. The OOK is the simple amplitude shift keying (ASK) modulation format and it has one bit in one symbol. The BPSK is the phase shift keying (PSK) method which uses two different phase values. Each of them represents one bit information, 0 or 1. The QPSK or 4QAM (2^MQAM where M is number of bits per symbol) uses four different phase values representing sequence of two bits. The QAM method modulates information in both of the phase and amplitude fields. However, the 8QAM code can be created in several forms, the one illustrated in Figure 1.5 (d) is the most common type. It has two amplitude values, each of it has four different phase

values. To increase capacity of network with growth of number of bits per symbol, 8QAM, 16QAM, 64QAM and other higher level modulation formats have been introduced.

1.2 Research Purpose

A structure of label router is illustrated in Figure 1.6. It performs several functions including label extraction, label recognition, switching, control signal generation, optical buffering and label swapping to process label. Some of the functions require electrical processing and it causes bottleneck issue. Moreover, it demands higher power consumption. Therefore, optical signal processing is expected for high speed packet switching network. Our research purpose is to implement label recognition function of the label router in optical domain.

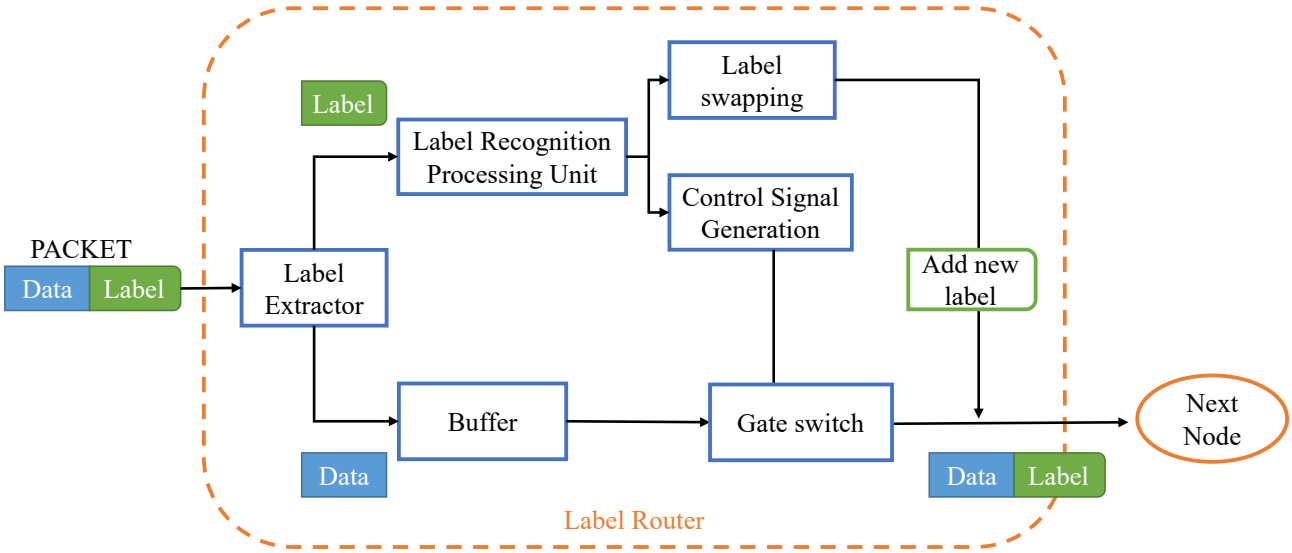

Figure 1.6: A structure of label router

So far, different kinds of methods have been investigated for optically coded label recognition. Optical correlator based systems with Fiber Bragg Grating [4], spatial filters [5]-[7] are popular way. However, in these systems, one correlator can recognize only one label. Therefore, required number of correlator is numerous for multiple labels. To recognize increased number of labels with single device, methods using Arrayed Waveguide Gratings (AWGs) [8], [9] have been reported. Our research group have been investigated simple recognition method using interference effect along passive waveguide circuits for binary phase shift keying (BPSK), quadrature phase shift keying (QPSK) and sixteen quadrature amplitude modulation (16QAM) coded label recognition [10]-[12].

In this work, we consider optical eight quadrature amplitude modulation (8QAM) coded label recognition with waveguide type recognition circuit on the basis of previous QPSK code identification method [11]. We examine operation of our proposed method by theoretical calculation and numerical simulation method.

1.3 Structure of the Thesis

This thesis consists of 8 chapters. In Chapter 1, research background and purpose are stated. Chapter 2 describes the waveguide types and its mathematical fundamentals. In Chapter 3, transmission parameters for signal quality measurement are explained. Chapter 4 discusses a basis of our proposed waveguide recognition circuit. In Chapter 5, a proposed recognition circuits for 1- and 2- symbol 8QAM code are explained with its theoretical results and FD-BPM simulation result for minimum output 1- symbol recognition circuit is demonstrated. In Chapter 6, noise tolerance for proposed methods is evaluated. A Chapter 7 summarizes our research work.

Chapter 2

Background of Optical Waveguide

An optical waveguide is a structure for guiding light along the direction of propagation. A well known waveguides are optical fiber and rectangular waveguides and they are used as a transmission medium in a communication network or as components of integrated optical circuits. Usually, a waveguide contains region called core with higher refractive index which is surrounded by lower refractive index cladding or substrate as shown in Figure 2.1. These refractive index difference confines light within the core and this effect can be understood by total internal reflection phenomena.

Optical waveguides are classified into several types depending on its geometry, mode structure and refractive index distribution. If the geometry is rectangular, it's called planar waveguide. While, the optical fiber is a circular type. For mode structure, relying on the electromagnetic field distribution, there are two independent electromagnetic modes named transverse electric (TE) and transverse magnetic (TM). In addition, number of modes or waves, which can be transmitted, defines whether it is a single-mode or a multi-mode structure. For refractive index distribution, if there is a step or abrupt changes between core and cladding refractive indexes, it is step-index waveguide. Whereas, if the core index is gradually decreases into its surface, it is graded-index. Upcoming sections in this chapter will explain about waveguide in more detail [13] $\sim$ [16].

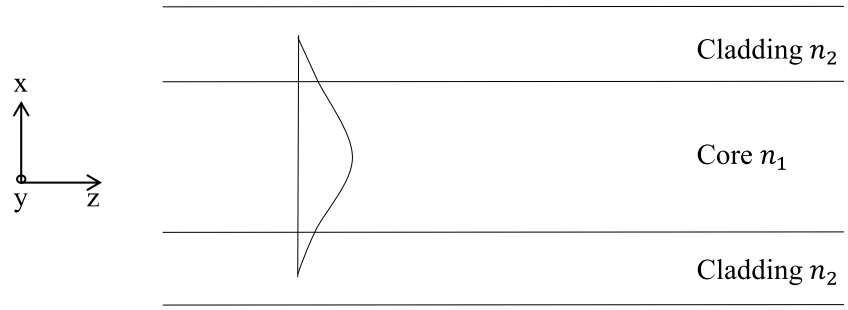

Figure 2.1: Basic structure of optical waveguide

2.1 Maxwell's Equations

Since the light is a electromagnetic waves, its propagation along the waveguide can be understood by Maxwell's equations.

Maxwell's Equations are a set of four partial differential equations that can describe how electric and magnetic fields propagate, interact, and how they are influenced by objects. These are,

$$\nabla \times \mathbf{E} = -\frac{\partial \mathbf{B}}{\partial t} \tag{2.1a}$$

$$\nabla \times \mathbf{H} = \frac{\partial \mathbf{D}}{\partial t} + \mathbf{J} \tag{2.1b}$$

$$\mathrm{div}\mathbf{D} = \rho \tag{2.1c}$$

$$\mathrm{div}\mathbf{B} = 0 \tag{2.1d}$$

where expression (2.1a) is Faraday's law, (2.1b) is Ampere's law, (2.1c) is Gauss's law, and (2.1d) is Gauss' Magnetism law. E[V/m] is electric field, H[A/m] is magnetic field, D[C/m^2] is electric flux density, B[T] is magnetic flux density, J[A/m^2] is current density and ρ[C/m^3] is electric charge density.

Here, the current density and the charge density satisfy the continuity equation.

$$\frac{\partial \rho}{\partial t} + \mathrm{div}\mathbf{J} = 0 \tag{2.2}$$

When polarization P[C/m^2] and magnetization M[A/m] exist in the medium, constituent equations can be written as follows,

$$\mathbf{D} = \varepsilon_0 \mathbf{E} + \mathbf{P} \tag{2.3a}$$

$$\mathbf{B} = \mu_0 \mathbf{H} + \mathbf{M} \tag{2.3b}$$

$$\mathbf{J} = \sigma \mathbf{E} \tag{2.3c}$$

$$\varepsilon_0 = 8.854 \times 10^{-12}[\mathrm{F/m}]$$

$$\mu_0 = 4\pi \times 10^{-7}[\mathrm{H/m}]$$

where σ is electric conductivity, ε_0 is permittivity in vacuum, and μ_0 is permeability in vacuum.

If electric and magnetic fields are negligible, polarization and magnetization can be expressed by following linear functions, where χ_E is electric susceptibility and χ_0 is magnetic susceptibility.

$$\mathbf{P} = \varepsilon_0 \chi_E \mathbf{E} \tag{2.4a}$$

$$\mathbf{M} = \mu_0 \chi_M \mathbf{H} \tag{2.4b}$$

When substituting Eq. (2.4) into (2.3), following two sets of equations, where ε is specific dielectric constant and μ is relative magnetic permeability, can be obtained.

$$\mathbf{D} = \varepsilon \varepsilon_0 \mathbf{E}, \qquad \varepsilon \equiv 1 + \chi_E \tag{2.5a}$$

$$\mathbf{B} = \mu \mu_0 \mathbf{H}, \qquad \mu \equiv 1 + \chi_M \tag{2.5b}$$

In the optical waveguide, by knowing the distribution of the refractive index, the electromagnetic field and other derived characteristic can be found. The refractive index n is directly related to the dielectric constant ε.

$$n^2 = \varepsilon \tag{2.6}$$

2.1.1 Boundary Conditions

In order to define electromagnetic field distribution within the waveguide, Maxwell's equation should be solved with boundary conditions referring walls or surfaces of the guide. The boundary condition is considered when the dielectric constants or refractive indexes of the waveguide mediums are different or discontinued as shown in Figure 2.1. At the boundary or core-cladding interface, both of the electric and magnetic tangential components must be continuous as expressed by

$$E_t^{(1)} = E_t^{(2)} \tag{2.7a}$$

$$H_t^{(1)} = H_t^{(2)} \tag{2.7b}$$

where t denotes the tangential components to the boundary and the superscripts (1) and (2) indicate the core and cladding regions, respectively. Besides it, there are other boundary conditions that require the electromagnetic fields to be zero at infinity and from this phenomena different types of electromagnetic modes are obtained.

2.2 Analysis of Optical Waveguide

The waveguide usually has three-dimensional (3D) structure as shown in Figure 2.2 (a). Although there are software and calculators that perform numerical analysis for 3D structure, it is complicated and takes long processing time. Therefore, to simplify it, waveguide is considered and approximated as a two dimensional (2D), called slab waveguide as shown in Figure 2.2 (b). Since in our research work, we analyze proposed recognition circuit in 2D model, we discuss about 2D waveguide in furthermore.

2.2.1 2D-slab waveguide

For 2D-slab waveguide as shown in Figure 2.1 or Figure 2.2 (b), the light wave propagation is taken at z direction. In this kind of structural waveguide, electromagnetic fields don't have y access dependency, so the partial differential in this direction is zero ($\partial E/\partial y = 0, \partial H/\partial y = 0$). Substituting this condition into Maxwell's equations, following expressions are derived.

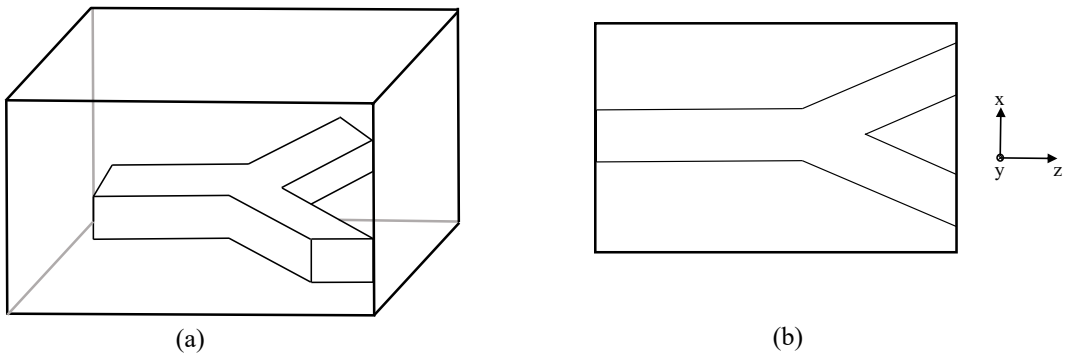

Figure 2.2: Waveguide structure (a) 3D waveguide structure, (b) 2D waveguide structure

$$-\frac{\partial E_y}{\partial z} + j\omega\mu H_x = 0 \tag{2.8a}$$

$$\frac{\partial E_x}{\partial z} - \frac{\partial E_z}{\partial x} + j\omega\mu H_y = 0 \tag{2.8b}$$

$$\frac{\partial E_y}{\partial x} + j\omega\mu H_z = 0 \tag{2.8c}$$

$$-j\omega\varepsilon E_x - \frac{\partial H_y}{\partial z} = 0 \tag{2.8d}$$

$$-j\omega\varepsilon E_y + \frac{\partial H_x}{\partial z} - \frac{\partial H_z}{\partial x} = 0 \tag{2.8e}$$

$$-j\omega\varepsilon E_z + \frac{\partial H_y}{\partial x} = 0 \tag{2.8f}$$

From here, two independent electromagnetic modes, TE and TM, can be be understood. For TE wave, the variable is often set to only E_y. By partially differentiating the Eq. (2.8a) and (2.8c) with z and x respectively and assigning them to the Eq. (2.8e), the expression for E_y is found. Firstly, by transforming Eq. (2.8 a) by leaving H_x at left side and partially differentiating both sides with z, the following equation is obtained.

$$\frac{\partial H_x}{\partial z} = \frac{\partial}{\partial z}(\frac{1}{j\omega\mu}\frac{\partial E_y}{\partial z}) = \frac{1}{j\omega\mu}\frac{\partial^2 E_y}{\partial z^2} \tag{2.9}$$

After that, deformation of Eq. (2.8c) by separating H_z at left side and other parameters at right side and differentiating both sides by x partially is expressed as

$$\frac{\partial H_z}{\partial x} = \frac{\partial}{\partial x}(\frac{-1}{j\omega\mu}\frac{\partial E_y}{\partial x}) = \frac{-1}{j\omega\mu}\frac{\partial^2 E_y}{\partial x^2}. \tag{2.10}$$

Substituting Eq. (2.9) and (2.10) into (2.8e)

$$\frac{1}{j\omega\mu}\frac{\partial^2 E_y}{\partial x^2} + \frac{1}{j\omega\mu}\frac{\partial^2 E_y}{\partial z^2} - j\omega\varepsilon E_y = 0 \tag{2.11}$$

is found. After multiplying both sides of Eq. (2.11) by $j\omega\mu$, it is derived as below.

$$\frac{\partial^2 E_y}{\partial x^2} + \frac{\partial^2 E_y}{\partial z^2} + \omega^2\varepsilon\mu E_y = 0 \tag{2.12}$$

If $\mu = \mu_0$

$$\omega^2\varepsilon\mu = \omega^2\varepsilon_0\mu_0\varepsilon_r = k_0^2 n^2 \tag{2.13}$$

, Eq. (2.12) can be rewritten as

$$\frac{\partial^2 E_y}{\partial x^2} + \frac{\partial^2 E_y}{\partial z^2} + k_0^2 n^2 E_y = 0 \tag{2.14}$$

where k_0 is the wavenumber in a vacuum, which represents rotation angle per meter, and it is equal with $2\pi/\lambda$. Eq. (2.14) is a basic wave equation for describing the TE mode where

each component is expressed by the followings.

$$H_x = \frac{1}{j\omega\mu}\frac{\partial E_y}{\partial z} \tag{2.15a}$$

$$H_z = \frac{-1}{j\omega\mu}\frac{\partial E_y}{\partial x} \tag{2.15b}$$

$$H_y = E_x = E_z = 0 \tag{2.15c}$$

From here, for TE wave, during propagation along the waveguide the electric field component is zero ($E_z = 0$) to the propagation direction z but it is perpendicular to it. Therefore, it is called transverse electric (TE) mode.

To express TM wave, Eq. (2.8d) is deformed by separating E_x at left side, and implementing partial differentiation on both sides by z as below.

$$E_x = \frac{-1}{j\omega\varepsilon}\frac{\partial H_y}{\partial z} = 0 \tag{2.16a}$$

$$\frac{\partial E_x}{\partial z} = \frac{\partial}{\partial z}(\frac{-1}{j\omega\varepsilon}\frac{\partial H_y}{\partial z}) = -\frac{1}{j\omega\varepsilon_0}\frac{\partial}{\partial z}(\frac{1}{n^2}\frac{\partial H_y}{\partial z}) \tag{2.16b}$$

Also, deforming the Eq. (2.8f) by leaving E_z at left side and partially differentiating both sides with x, we get following equation.

$$E_z = \frac{1}{j\omega\varepsilon}\frac{\partial H_y}{\partial x} = 0 \tag{2.17a}$$

$$\frac{\partial E_z}{\partial x} = \frac{\partial}{\partial x}(\frac{1}{j\omega\varepsilon}\frac{\partial H_y}{\partial x}) = \frac{1}{j\omega\varepsilon_0}\frac{\partial}{\partial x}(\frac{1}{n^2}\frac{\partial H_y}{\partial x}) \tag{2.17b}$$

If we substitute Eq. (2.16b) and (2.17b) into (2.8b)

$$\frac{-1}{j\omega\varepsilon_0}\frac{\partial}{\partial x}(\frac{1}{n^2}\frac{\partial H_y}{\partial x}) + \frac{-1}{j\omega\varepsilon_0}\frac{\partial}{\partial z}(\frac{1}{n^2}\frac{\partial H_y}{\partial z}) + j\omega\mu H_y = 0 \tag{2.18}$$

and multiple both sides by $-j\omega\varepsilon_0$, we get

$$\frac{\partial}{\partial x}(\frac{1}{n^2}\frac{\partial H_y}{\partial x}) + \frac{\partial}{\partial z}(\frac{1}{n^2}\frac{\partial H_y}{\partial z}) + \omega^2\mu\varepsilon_0 H_y = 0. \tag{2.19}$$

Then, substitute $\omega^2\mu_0\varepsilon_0 = k_0^2(\mu = \mu_0, k_0 = 2\pi/\lambda)$ into Eq. (2.19), we get the following basic equation for TM wave.

$$\frac{\partial}{\partial x}(\frac{1}{n^2}\frac{\partial H_y}{\partial x}) + \frac{\partial}{\partial z}(\frac{1}{n^2}\frac{\partial H_y}{\partial z}) + k_0^2 H_y = 0 \tag{2.20}$$

Each of the components can be expressed by belows.

$$E_x = \frac{-1}{j\omega\varepsilon_0 n^2}\frac{\partial H_y}{\partial z} \tag{2.21a}$$

$$E_z = \frac{1}{j\omega\varepsilon_0 n^2}\frac{\partial H_y}{\partial x} \tag{2.21b}$$

$$E_y = H_x = H_z = 0 \tag{2.21c}$$

From these expressions, it can be concluded that magnetic field along the z axis is zero ($H_z = 0$). Therefore, the magnetic field to the propagation direction is perpendicular and it is called transverse magnetic (TM) mode.

Ignoring the derivative with respect to the refractive index n, the formulas of TE and TM wave have the same shape. In the field of waveguide analysis, the relative refractive index is used as an amount representing the refractive index difference between the core and the cladding. The definition of relative refractive index is given by the following equation

$$\triangle = \frac{n_1^2 - n_0^2}{2n_1^2} \tag{2.22}$$

where n_0 is the cladding, and n_1 is the core refractive index. When the relative refractive index is small, the following approximation is used.

$$\triangle = \frac{n_1^2 - n_0^2}{2n_1^2} \simeq \frac{n_1 - n_0}{n_1} \tag{2.23}$$

In case of a waveguide with a small relative refractive index, since the value of differential term of the refractive index is small, TE and TM waves exhibit substantially the same characteristics. Therefore, it is also possible to approximate the TM wave with the TE wave.

TE mode in 2D slab waveguide

Because in our work, we analyze TE mode propagation along our proposed waveguide circuit, we would like to extend its characteristics in more detail. We consider the guided electromagnetic fields are confined in the core and exponentially decay in the cladding in a slab waveguide as shown in Figure 2.3. As explained before, TE mode can be expressed by Eq. (2.14) and (2.15). E_y, H_x, H_z are the complex functions with respect to the x and z. From Eq. (2.14) and (2.15a), E_y can be solved. However, at the boundary between core and clad, the components in contact with the interface must be continuous. So, E_y and H_z must be considered together.

If there is a solution in a separated form, we obtain $E_y(x, z) = \phi(x)e^{-j\beta z}$. Here, β is a real number. Since $\mid e^{-j\beta z} \mid = 1$, this solution does not increase or decrease and represents

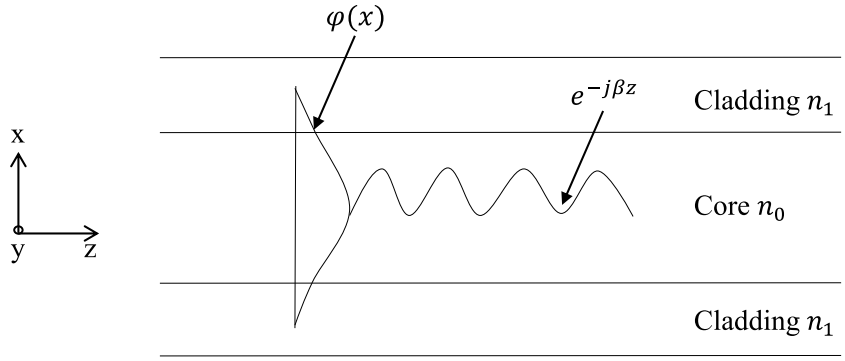

Figure 2.3: Guided mode along waveguide

a wave that continuously propagate in the z direction as shown in Figure 2.3. Substituting

$E_y(x,z) = \phi(x)e^{-j\beta z}$ into Eq. (2.15), because the first derivative in the z direction is replaced by multiplication of $-j\beta$,

$$\frac{\partial^2 E_y}{\partial z^2} = -\beta^2 E_y \tag{2.24}$$

and then following equation is obtained.

$$\frac{\partial^2}{\partial x^2}(\phi e^{-j\beta z}) - \beta^2 \phi e^{-j\beta z} + k_0^2 n^2 \phi e^{-j\beta z} = 0 \tag{2.25}$$

Here, when both sides are divided by $e^{-j\beta z}$, it is rewritten as

$$\frac{\partial^2 \phi}{\partial x^2} + (k_0^2 n^2 - \beta^2)\phi = 0. \tag{2.26}$$

At this point, β is undetermined. Only when β takes a specific value, $\phi(x)e^{-j\beta z}$ can satisfy the Eq. (2.14) and the following two boundary conditions.

1. Since it represents the light waves propagating along the waveguide, the fields E_y, H_x, H_z are 0 at $x = \pm\infty$ which is a location far from the waveguide.

2. The tangential components of the electromagnetic field (E_y and H_z) are continuous at the interface between core and cladding. From Eq.(2.15b), it can be seen that H_z is proportional to the y-direction and E_y and $\partial Ey/\partial x$ are continuous at the boundary.

For expression $E_y(x,z) = \phi(x)e^{-j\beta z}$, the boundary conditions are:

1. $\phi(x)$ is 0 at $x = \pm\infty$.

2. ϕ and $\partial\phi/\partial x$ are continuous at the boundary between core and cladding. ϕ must satisfy this condition and partial differential equation expressed by Eq. (2.26).

The refractive index takes a constant value of n_0 for core and n_1 for cladding. Therefore, analytical solution of Eq. (2.26) for three regions as shown in Figure 2.3 can be found. The solution varies with the sign of $k_0^2 n^2 - \beta^2$.

$$k_0^2 n^2 - \beta^2 > 0 : \phi = A cos\alpha x + B sin\alpha x \tag{2.27a}$$

$$k_0^2 n^2 - \beta^2 < 0 : \phi = Ce^{\alpha x} + De^{-\alpha x} \tag{2.27b}$$

Here, in order to represent it in a unified way without separation, following expression is used

$$a = \sqrt{\beta^2 - k_0^2 n^2} \tag{2.28}$$

and if the inside of the radical is negative and the imaginary number is introduced, the solution of Eq. (2.26) can be written as

$$\phi(x) = Ae^{ax} + Be^{-ax}. \tag{2.29}$$

However, when a is an imaginary number, the coefficients A and B are complex numbers conjugating with each other. ϕ and $\partial\phi/\partial x$ in each layer of the waveguide is expressed as followings.

For the upper cladding:

$$\phi(x) : A_1 e^{\gamma x} + B_1 e^{-\gamma x} \tag{2.30a}$$

$$\frac{\partial\phi}{\partial x} : A_1\gamma e^{\gamma x} + B_1\gamma e^{-\gamma x} \tag{2.30b}$$

For core:

$$\phi(x) : A_2 e^{\kappa x} + B_2 e^{-\kappa x} \tag{2.31a}$$

$$\frac{\partial \phi}{\partial x} : A_2 \kappa e^{\kappa x} + B_2 \kappa e^{-\kappa x} \tag{2.31b}$$

For lower cladding:

$$\phi(x) : A_3 e^{\gamma x} + B_3 e^{-\gamma x} \tag{2.32a}$$

$$\frac{\partial \phi}{\partial x} : A_3 \gamma e^{\gamma x} + B_3 \gamma e^{-\gamma x} \tag{2.32b}$$

Here, k and γ are wavenumbers along the x-axis in the core and cladding regions and are given by:

$$\kappa = \sqrt{\beta^2 - k_0^2 n_1^2} \tag{2.33a}$$

$$\gamma = \sqrt{\beta^2 - k_0^2 n_0^2}. \tag{2.33b}$$

Although the k and γ are defined, the β is unknown and its possible range should be considered. In order to satisfy the boundary condition, ϕ must be a sine function in the core region and an exponential function in the cladding region. It means, $k_0 n_0 < \beta < k_0 n_1$ or $n_0 < \beta/k_0 < n_1$ must be satisfied. Here, β/k_0 is dimensionless value and is a refractive index for the plane wave called effective index and can be expressed as

$$n_{eff} = \beta/k_0. \tag{2.34}$$

The number of solutions depends on the width of the waveguide, the wavelength of light, the relative refractive index difference $\triangle = (n_1^2 - n_0^2)/(2n_1^2) \simeq (n_1 - n_0)/n_1$ and has the following properties.

1. For symmetric waveguide with same refractive index distribution in cladding regions, there can be one or more modes. For an asymmetric waveguide, there may be no mode at all.

2. The number of modes increases as the width of the waveguide increases.

3. The number of modes increases as the relative refractive index difference between the core and the clad increases.

A Figure 2.4 shows electric field distributions for some of the TE modes as an example.

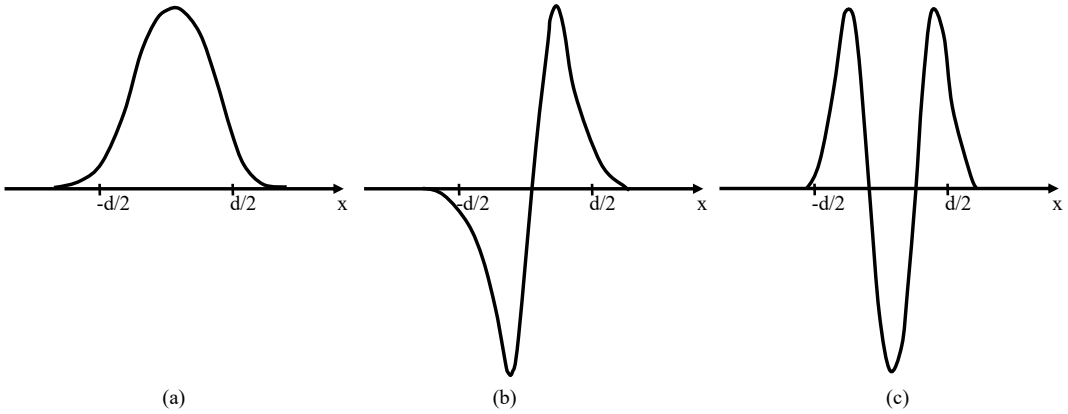

Figure 2.4: (a) TE_0 mode, (b) TE_1 mode, and (c) TE_2 mode

2.3 Optical Waveguide Analyzing Methods

As previously mentioned, 3D waveguide can be considered as 2D for analyzing purpose. It can be achieved with various methods as mentioned here briefly. The simplest one is effective index method which can be applicable to simple structure waveguide such as ridge and diffused guides. It makes assumption by expressing electromagnetic field with separation of variables. Depending on the waveguide structure, if the assumption of the separation of variables are not well defined, the accuracy of this technique becomes poor. Moreover, its usage for graded index or more complex structure waveguide is not quite efficient. To improve this limitation, another technique called Finite Element Method (FEM) is introduced. This method solves the problem by approximating discretized small elements and integrates solution of small elements for entire domain.

In integrated optical circuit, a curved, a branch, combining and S-shaped waveguides are commonly used to make connection of elements. To analyze such kind of guides, Beam Propagation Method (BPM) is proper one. It has two popular versions called Fast Fourier Transform Beam Propagation Method (FFT-BPM) and Finite Difference Beam Propagation Method (FD-BPM). Even though both of them have its own merits and demerits, FD-BPM is assessed that it has more accuracy, computational efficiency, and stability [17]. In this work, we use FD-BPM technique which calculates Maxwell's equations by using refractive index distribution of the waveguide as a parameter.

2.3.1 Finite Difference Beam Propagation Method

In order to solve the propagation problem of the field using FD-BPM, it is necessary to derive fundamental wave equation. Here we take the triple-layered symmetrical slab waveguide illustrated in Figure 2.5 as an example. In previous sections, it is considered that the wave propagation at direction z is uniform and is perpendicular to y axis. In FD-BPM, waveguide structure is considered to be non-uniform for z direction and it gradually changes.

The wave equation for TE mode is given by below expression as explained before.

$$\frac{\partial^2 E_y}{\partial z^2} + \frac{\partial^2 E_y}{\partial x^2} + k_0^2 \varepsilon_r E_y = 0 \tag{2.35}$$

Where k_0 is the wave number in a vacuum and $\varepsilon_r = n^2(x)$ is the relative permittivity along x

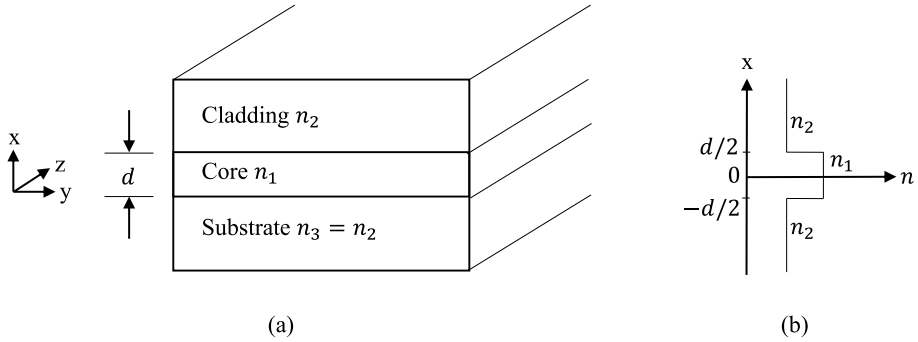

Figure 2.5: (a) Symmetrical slab waveguide, (b) Refractive index profile of slab waveguide

direction. To solve problem using FD-BPM, gradually changed problem region is divided into uniform small meshes. An approximation that divides wave function $E_y(x, y, z)$ propagating in the z direction into an amplitude term $\phi(x, y, z)$ that gradually changes in the traveling direction and a phase term $\exp(-i\beta z)$ vibrating violently as expressed by

$$E_y(x, y, z) = \phi(x, y, z) \exp(-i\beta z) \tag{2.36}$$

where $\beta = n_{eff} k_0$ and n_{eff} is effective refractive index.

Second order differentiation of Eq. (2.36) can be found as

$$\frac{\partial^2 E_y}{\partial z^2} = \frac{\partial^2 \phi}{\partial z^2} \exp(-i\beta z) - 2i\beta \frac{\partial \phi}{\partial z} \exp(-i\beta z) - \beta^2 \phi \exp(-i\beta z) \tag{2.37}$$

and substituting it into Eq. (2.35)

$$\frac{\partial^2 \phi}{\partial z^2} - 2i\beta \frac{\partial \phi}{\partial z} + \frac{\partial^2 \phi}{\partial x^2} + (k_0^2 \varepsilon - \beta^2)\phi = 0 \tag{2.38}$$

and separate it by exponential functional terms, we get following form.

$$2i\beta \frac{\partial \phi}{\partial z} - \frac{\partial^2 \phi}{\partial z^2} = \frac{\partial^2 \phi}{\partial x^2} + k_0^2 (\varepsilon - n_{eff}^2)\phi \tag{2.39}$$

If we ignore the second term of the Eq. (2.39) ($\partial^2 \phi / \partial z^2 = 0$), we obtain an approximation called Paraxial or Fresnel approximation written as

$$2i\beta \frac{\partial \phi}{\partial z} = \frac{\partial^2 \phi}{\partial x^2} + k_0^2 (\varepsilon - n_{eff}^2)\phi. \tag{2.40}$$

Here, for simplicity, Fresnel approximation is formulated. By making discretization for x and z coordinates

$$x = p\Delta x \tag{2.41a}$$
$$z = l\Delta z \tag{2.41b}$$

and abbreviating the wave function $\phi(x, z)$ and the relative permitivity $\varepsilon(x, z)$ we get

$$\phi(x, z) = \phi(p\Delta x, l\Delta z) \rightarrow \phi_p^l \tag{2.42a}$$
$$\varepsilon(x, z) = \varepsilon(p\Delta x, l\Delta z) \rightarrow \varepsilon_p^l \tag{2.42b}$$

where Δx and Δz denote the calculation steps in corresponding directions and p and l express the number of divisions along the x and z axis, respectively. Then let's discretize Eq. (2.40) only for x direction by discarding the l representing z direction for a while.

$$\frac{\partial^2\phi}{\partial x^2} = \frac{1}{\Delta x}\left\{\underbrace{\frac{\phi_{p+1}-\phi_p}{\Delta x}}_{Sp+\frac{1}{2}} - \underbrace{\frac{\phi_p-\phi_{p-1}}{\Delta x}}_{Sp-\frac{1}{2}}\right\} = \underbrace{\frac{\phi_{p+1}-2\phi_p+\phi_{p-1}}{(\Delta x)^2}}_{Sp} \tag{2.43a}$$

$$k_0^2(\varepsilon - n_{eff}^2)\phi = \underbrace{k_0^2(\varepsilon_p - n_{eff}^2)\phi_p}_{Sp} \tag{2.43b}$$

Substituting Eq. (2.43) into (2.40) we get

$$\begin{aligned} 2i\beta\frac{\partial\phi_p}{\partial z} &= \frac{\phi_{p+1}-2\phi_p+\phi_{p-1}}{(\Delta x)^2} + k_0^2(\varepsilon_p - n_{eff}^2)\phi_p \\ &= \alpha_w\phi_{p-1} + \alpha_x\phi_p + \alpha_e\phi_{p+1} + k_0^2(\varepsilon_p - n_{eff}^2)\phi_p. \end{aligned} \tag{2.44}$$

it can be rewritten as

$$2i\beta\frac{\partial\phi_p}{\partial z} = \alpha_w\phi_{p-1} + \left\{\alpha_x + k_0^2(\varepsilon_p - n_{eff}^2)\right\}\phi_p + \alpha_e\phi_{p+1} \tag{2.45}$$

where

$$\alpha_w = \frac{1}{(\Delta x)^2} \tag{2.46a}$$

$$\alpha_e = \frac{1}{(\Delta x)^2} \tag{2.46b}$$

$$\alpha_x = -\frac{2}{(\Delta x)^2}. \tag{2.46c}$$

If we differentiate left side of the Eq. (2.45) with respect to the coordinate z, the following expression is found.

$$2i\beta\frac{\partial\phi_p}{\partial z} \to 2i\beta\frac{\phi_p^{l+1}-\phi_p^l}{\Delta z} \tag{2.47}$$

It can be seen from above equation that with respect to the z on the left side of the Eq. (2.45) central difference between l and $l+1$ is $l+1/2$. Therefore, central difference for right side of the expression is $l+1/2$ and we get

$$\begin{aligned} 2i\beta\frac{\phi_p^{l+1}-\phi_p^l}{\Delta z} &= \frac{1}{2}\left[\alpha_w^l\phi_{p-1}^l + \left\{\alpha_x^l + k_0^2(\varepsilon_p^l - n_{eff}^2)\right\}\phi_p^l + \alpha_e^l\phi_{p+1}^l\right] \\ &+\frac{1}{2}\left[\alpha_w^{l+1}\phi_{p-1}^{l+1} + \left\{\alpha_x^{l+1} + k_0^2(\varepsilon_p^{l+1} - n_{eff}^2)\right\}\phi_p^{l+1} + \alpha_e^{l+1}\phi_{p+1}^{l+1}\right]. \end{aligned} \tag{2.48}$$

Here, if we summarize the term $l+1$ on the left side and the term l on the right side, it will be rewritten as

$$\begin{aligned} -\alpha_w^{l+1}\phi_{p-1}^{l+1} + \left\{-\alpha_x^{l+1} + \frac{4i\beta}{\Delta z} - k_0^2(\varepsilon_p^{l+1} - n_{eff}^2)\right\}\phi_p^{l+1} - \alpha_e^{l+1}\phi_{p+1}^{l+1} \\ = \alpha_w^l\phi_{p-1}^l + \left\{\alpha_x^l + \frac{4i\beta}{\Delta z} + k_0^2(\varepsilon_p^l - n_{eff}^2)\right\}\phi_p^l + \alpha_e^l\phi_{p+1}^l. \end{aligned} \tag{2.49}$$

The main field H_y of the TM mode also can be expressed like above equation. In that case we use following expressions instead of Eq. (2.46).

$$\alpha_w = \frac{1}{(\Delta x)^2}\frac{2\varepsilon_p}{\varepsilon_p+\varepsilon_{p-1}} \tag{2.50a}$$

$$\alpha_e = \frac{1}{(\Delta x)^2}\frac{2\varepsilon_p}{\varepsilon_p+\varepsilon_{p+1}} \tag{2.50b}$$

$$\alpha_x = -\frac{1}{(\Delta x)^2}\frac{2\varepsilon_p}{\varepsilon_p+\varepsilon_{p-1}} - \frac{1}{(\Delta x)^2}\frac{2\varepsilon_p}{\varepsilon_p+\varepsilon_{p+1}} = -\alpha_w - \alpha_e \tag{2.50c}$$

2.3.2 Stability Condition

Previously, the central difference for left side of the Eq. (2.40) has been defined. Similarly, the central difference on the right side can be expressed as the intermediate point $z+\Delta z/2$ between z and $z+\Delta z$. Here, taking the Fresnel equation as an example, we will consider the difference center on the right side and the stability during beam propagation. Assume a uniform medium for simplicity. Therefore, if $n_{eff}^2=\varepsilon$, Eq. (2.40) written as below.

$$2i\beta\frac{\partial\phi}{\partial z} = \frac{\partial^2\phi}{\partial x^2} \tag{2.51}$$

By deriving the z direction of Eq. (2.51) we introduce the parameter α which determines the central difference.

$$2i\beta\frac{\phi(z+\Delta z)-\phi(z)}{\Delta z} = \alpha\frac{\partial^2\phi(z+\Delta z)}{\partial x^2} + (1-\alpha)\frac{\partial^2\phi(z)}{\partial x^2} \tag{2.52}$$

Here, the case of $\alpha=0.5$ corresponds to the Eq. (2.48), which is called the Crank-Nicolson method.

Next, the influence of a parameter α on the stability of calculation result is investigated.

$$\phi(z) = \phi_0\exp(ik_x x)\exp(-i\beta z) \tag{2.53}$$

Assuming a plane wave as a moderately changing wave function, we obtain

$$\frac{\partial^2\phi(z)}{\partial x^2} = -k_x^2\phi(z). \tag{2.54}$$

After substituting Eq. (2.53) into (2.54) and then dividing by ϕ we get following expression.

$$\begin{aligned} 2i\beta\frac{1}{\Delta z}(\exp(-i\beta z)-1) &= -k_x^2\left\{\alpha\exp(-i\beta\Delta z)+(1-\alpha)\right\} \\ \left(\frac{2i\beta}{\Delta z}+k_x^2\alpha\right)\exp(-i\beta z) &= \frac{2i\beta}{\Delta z}-(1-\alpha)k_x^2 \\ \exp(-i\beta z) &= \frac{\frac{2i\beta}{\Delta z}-(1-\alpha)k_x^2}{\frac{2i\beta}{\Delta z}+\alpha k_x^2} \end{aligned} \tag{2.55}$$

Since above equation defines a propagation term, by examining the change of its absolute value λ with respect to the propagation distance z, it is possible to investigate the relationship between parameter α and stability at the same time during beam propagation.

$$\begin{aligned}\lambda &= |\exp(-i\beta\Delta z)| \\ &= \left\{\frac{\left(\frac{2\beta}{\Delta z}\right)^2 + (1-\alpha)^2 k_x^4}{\left(\frac{2\beta}{\Delta z}\right)^2 + \alpha^2 k_x^4}\right\}^{\frac{1}{2}} \\ &= \left\{\frac{C^2 + (1-\alpha)^2 k_x^4}{C^2 + \alpha^2 k_x^4}\right\} \end{aligned} \tag{2.56}$$

If $C = 2\beta/\Delta z$, it can be written in following three forms depending on the value of parameter α.

(1) $\alpha = 0.5$

$$\lambda = \left\{\frac{C^2 + k_x^4/4}{C^2 + k_x^4/4}\right\}^{\frac{1}{2}} = 1 \tag{2.57}$$

(2) $0.5 < \alpha \leq 1$ **and** $(1-\alpha)^2 < \alpha^2$

$$\lambda = \left\{\frac{C^2 + (1-\alpha)^2 k_x^4}{C^2 + \alpha^2 k_x^4}\right\}^{\frac{1}{2}} < 1 \tag{2.58}$$

For this case, although the field is always stable, it decays with propagation.

(3) $0 \leq \alpha < 0.5$ **and** $(1-\alpha)^2 > \alpha^2$

$$\lambda = \left\{\frac{C^2 + (1-\alpha)^2 k_x^4}{C^2 + \alpha^2 k_x^4}\right\}^{\frac{1}{2}} > 1 \tag{2.59}$$

For this case, the field increases and diverges with propagation.

As described above, the value of parameter α should be at least $\alpha = 0.5$. If we follow this condition, Eq. (2.48) is rewritten as below.

$$\begin{aligned} 2i\beta\frac{\phi_p^{l+1} - \phi_p^l}{\Delta z} &= \alpha\left[\alpha_w^l \phi_{p-1}^l + \left\{\alpha_x^l + k_0^2(\varepsilon_p^l - n_{eff}^2)\right\}\phi_p^l + \alpha_e^l \phi_{p+1}^l\right] \\ &\quad +(1-\alpha)\left[\alpha_w^{l+1}\phi_{p-1}^{l+1} + \left\{\alpha_x^{l+1} + k_0^2(\varepsilon_p^{l+1} - n_{eff}^2)\right\}\phi_p^{l+1} + \alpha_e^{l+1}\phi_{p+1}^{l+1}\right] \end{aligned} \tag{2.60}$$

The specific way of solving this equation is same as the Crank-Nicholson method.

2.3.3 Transparent Boundary Conditions

For accurate numerical analysis, an infinite wide area with no reflection can not be applied as an analyzing area. So a finite area needs to be considered. Because in the presence of a radiation field, it is reflected from the boundary of the analyzing area and returns to the vicinity of the core region. Then it interacts with the guided light and deteriorates the calculation accuracy. In this section, we describe the transparent boundary condition (TBC) proposed by Hadley. A purpose of the TBC is to efficiently remove the reflection from the

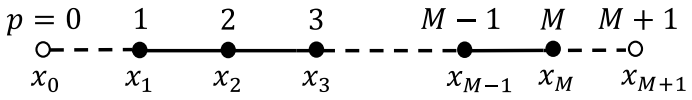

Figure 2.6: Regions of waveguide

analyzing boundary. Although a two-dimensional problem is described here, it can be easily extended to a three-dimensional problem.

As shown in Figure 2.6, analyzing region is assumed within $p = 1$ to M. So, $p = 0$ and $M + 1$ represent an area outside of the analyzing region, and we will consider it.

(1) Left hand boundary

Here, we discuss area between the node $p = 0$ which is outside of the boundary and the node $p = 1$ on the boundary. At the left end of the analysis region, consider the next traveling wave with wave number k_x is going to the left.

$$\phi(x, z) = A(z) \exp(ik_x x) \tag{2.61}$$

Let x coordinates at nodes $p = 0, 1, 2$ be x_0, x_1, x_2 and wave functions ϕ_0, ϕ_1, ϕ_2

$$\phi_0 = A(z) \exp(ik_x x_0) \tag{2.62a}$$
$$\phi_1 = A(z) \exp(ik_x x_1) \tag{2.62b}$$
$$\phi_2 = A(z) \exp(ik_x x_2) \tag{2.62c}$$

Here, ϕ_1 and ϕ_2 are wave functions existing in the analyzing region, and ϕ_0 is a wave function outside of the analyzing region to cause influence. If we divide Eq. (2.62c) by (2.62b) and (2.62b) by (2.62a), we get

$$\exp(ik_x \Delta x) = \phi_2/\phi_1 \tag{2.63a}$$
$$\exp(ik_x \Delta x) = \phi_1/\phi_0 \tag{2.63b}$$

where $\Delta x = x_2 - x_1 = x_1 - x_0$ is used. Therefore, we obtain below from Eq. (2.63a)

$$\eta_1 = \phi_2/\phi_1 \tag{2.64}$$

and assigning it into Eq. (2.63b) we get

$$\phi_0 = \phi_1/\eta_1. \tag{2.65}$$

On the other hand following expression can be obtained from Eq. (2.63a)

$$k_x = \frac{1}{i\Delta x} \ln(\eta_1) \tag{2.66}$$

and substituting it into (2.63b) we get

$$\phi_0 = \phi_1 \exp(-ik_x \Delta x). \tag{2.67}$$

In this case, $Re(kx) > 0$ because it is a wave traveling to the left. If $Re(kx) < 0$, there will be a reflection from the boundary and it is necessary to change the sign of $Re(kx)$.

(2) Right hand boundary

Here we discuss the region between node $p = M + 1$, which is outside of the boundary and node $p = M$, which is on the boundary. At left end of the analyzing region, consider the next traveling wave with wave number k_x is going to the right.

$$\phi(x, z) = A(z) \exp(-ik_x x) \tag{2.68}$$

Let x_{M-1}, x_M, x_{M+1} be the x coordinates and $\phi_{M-1}, \phi_M, \phi_{M+1}$ be the wave functions at nodes $p = M - 1, M, M + 1$. The wave functions are expressed by below equations.

$$\begin{aligned} \phi_{M-1} &= A(z) \exp(-ik_x x_{M-1}) && \text{(2.69a)} \\ \phi_M &= A(z) \exp(-ik_x x_M) && \text{(2.69b)} \\ \phi_{M+1} &= A(z) \exp(-ik_x x_{M+1}) && \text{(2.69c)} \end{aligned}$$

Here, ϕ_{M-1} and ϕ_M are wave functions existing in the analyzing region and ϕ_{M+1} is a wave function outside of the analyzing region. From the divisions of Eq. (2.69c) / (2.69b) and (2.69b) / (2.69a), we obtain

$$\begin{aligned} \exp(-ik_x \Delta x) &= \phi_{M+1}/\phi_M && \text{(2.70a)} \\ \exp(-ik_x \Delta x) &= \phi_M/\phi_{M-1} && \text{(2.70b)} \end{aligned}$$

Here, $\Delta x = x_M - x_{M-1} = x_{M+1} - x_M$ was used. Therefore, from Eq. (2.70b) we can define below expression

$$\eta_M = \phi_M/\phi_{M-1} \tag{2.71}$$

and assign it to Eq. (2.69a) we get

$$\phi_{M+1} = \phi_M \eta_M. \tag{2.72}$$

We obtain below expression from Eq. (2.69b)

$$k_x = \frac{1}{-i\Delta x} \ln(\eta_M) \tag{2.73}$$

and then substituting it into Eq. (2.70a), following expression can be found.

$$\phi_{M+1} = \phi_M \exp(-ik_x \Delta x) \tag{2.74}$$

In this case, $Re_{(kx)} > 0$ because it is a wave traveling to the right. If $Re_{(kx)} < 0$, it is necessary to replace the sign of $Re_{(kx)}$ like the left boundary.

2.4 Programming Numerical Method

In this section, we explain how to program numerical method with transparent boundary condition. The most widely used technique is Crank-Nicholson method. Suppose we know

the field ϕ^l at the coordinate z (suffix is l) and we want to find the field ϕ^{l+1} at the coordinate $z+\Delta z$ (subscript is $l+1$). From equation (2.49) we can define

$$-\alpha_w^{l+1}\phi_{p-1}^{l+1}+\left\{-\alpha_x^{l+1}+\frac{4i\beta}{\Delta z}-k_0^2(\varepsilon_p^{l+1}-n_{eff}^2)\right\}\phi_p^{l+1}-\alpha_e^{l+1}\phi_{p+1}^{l+1}$$
$$=\alpha_w^l\phi_{p-1}^l+\left\{\alpha_x^l+\frac{4i\beta}{\Delta z}+k_0^2(\varepsilon_p^l-n_{eff}^2)\right\}\phi_p^l+\alpha_e^l\phi_{p+1}^l. \tag{2.75}$$

$\phi_{p-1}^{l+1},\phi_p^{l+1},\phi_{p+1}^{l+1}$ at left side of this equation are exponent boundary that we are seeking at $z+\Delta z$ coordinate. $\phi_{p-1}^l,\phi_p^l,\phi_{p+1}^l$ are known boundary at coordinate z. Here, p is assumed to be $p=1\sim M$. Then, if we put following coefficients

$$A(p) = -\alpha_w^{l+1} \tag{2.76a}$$
$$B(p) = \left\{-\alpha_x^{l+1}+\frac{4i\beta}{\Delta z}-k_0^2(\varepsilon_p^{l+1}-n_{\text{eff}}^2)\right\} \tag{2.76b}$$
$$C(p) = -\alpha_e^{l+1} \tag{2.76c}$$
$$D(p) = \alpha_w^l\phi_{p-1}^l+\left\{\alpha_x^l+\frac{4i\beta}{\Delta z}+k_0^2(\varepsilon_p^l-n_{\text{eff}}^2)\right\}\phi_p^l+\alpha_e^l\phi_{p+1}^l \tag{2.76d}$$

into Equation (2.75), it will be simplified as below form.

$$A(p)\phi_{p-1}^{l+1}+B(p)\phi_p^{l+1}+C(p)\phi_{p+1}^{l+1}=D(p) \tag{2.77}$$

We can transform Equation (2.77) as followings at the left and right end node of the analyzing region to consider the transparent boundary condition.

(1) The leftmost point $(p=1)$

The boundary ϕ_1 of the left end point is affected by the boundary ϕ_0 of the node outside of the analyzing region. From equation (2.65)

$$\phi_0=\phi_1\gamma_L,\quad \gamma_L=1/\eta_1=\phi_1^l/\phi_2^l \tag{2.78}$$

is obtained. γ_L is determined from the boundary of l. Therefore, Equation (2.77) becomes

$$B'(1)\phi_1^{l+1}+C(1)\phi_2^{l+1}=D(1). \tag{2.79}$$

Here, each coefficient is expressed by

$$B'(1) = -\alpha_w^{l+1}\gamma_L+\left\{-\alpha_x^{l+1}+\frac{4i\beta}{\Delta z}-k_0^2(\varepsilon_1^{l+1}-n_{\text{eff}}^2)\right\} \tag{2.80a}$$
$$C(1) = -\alpha_e^{l+1} \tag{2.80b}$$
$$D(1) = \alpha_w^l\gamma_L\phi_1^l+\left\{\alpha_x^l+\frac{4i\beta}{\Delta z}+k_0^2(\varepsilon_1^l-n_{\text{eff}}^2)\right\}\phi_1^l+\alpha_e^l\phi_2^l. \tag{2.80c}$$

(2) The rightmost point $(p=M)$

The boundary ϕ_M of the rightmost point is affected by the ϕ_{M+1} outside of the analysis region. So, Equation (2.72) is rewritten as

$$\phi_{M+1} = \phi_M \gamma_R, \quad \gamma_R = \eta_M = \phi_M^l / \phi_{M-1}^l \tag{2.81}$$

where γ_R is determined from the boundary of l. So, expression (2.77) becomes

$$A(M)\phi_{M-1}^{l+1} + B'(M)\phi_M^{l+1} = D(M). \tag{2.82}$$

Here, the coefficients in Eq. (2.82) are expressed by followings respectively.

$$A(M) = -\alpha_w^{l+1} \tag{2.83a}$$

$$B'(M) = -\alpha_e^{l+1}\gamma_R + \left\{ -\alpha_x^{l+1} + \frac{4i\beta}{\Delta z} - k_0^2(\varepsilon_M^{l+1} - n_{\text{eff}}^2) \right\} \tag{2.83b}$$

$$D(M) = \alpha_w^l \phi_{M-1}^l + \left\{ \alpha_e^l \gamma_R + \alpha_x^l + \frac{4i\beta}{\Delta z} + k_0^2(\varepsilon_M^l - n_{\text{eff}}^2) \right\} \phi_M^l \tag{2.83c}$$

Therefore, when we put them together into matrix form, it is expressed as

$$\begin{pmatrix} B'(1) & C(1) & & & & \\ A(2) & B(2) & C(2) & & & \\ & A(3) & B(3) & C(3) & & \\ & & \ddots & \ddots & & \\ & & & \ddots & C(M-1) \\ & & & A(M) & B'(M) \end{pmatrix} \begin{pmatrix} \phi_1^{l+1} \\ \phi_2^{l+1} \\ \phi_3^{l+1} \\ \vdots \\ \phi_{M-1}^{l+1} \\ \phi_M^{l+1} \end{pmatrix} = \begin{pmatrix} D(1) \\ D(2) \\ D(3) \\ \vdots \\ D(M-1) \\ D(M) \end{pmatrix}. \tag{2.84}$$

Equation (2.84) has a trilateral diagonal shape, and if a methods such as Thomas method are used, unknown wave functions $\phi_1^{l+1} \sim \phi_M^{l+1}$ can be efficiently obtained.

2.5 Wide Angle Analysis with Padé Approximation Operator

So far, we have considered the Fresnel equation based techniques. Here we describe the wide-angle (WA) beam propagation method using the Padé approximation operator and multi-step method proposed by Hadley in order to improve accuracy and efficiency of beam propagation method. Wide-angle expression omits the second-order differentiation with respect to z of the wave function expressed by Eq. (2.39) and written as

$$2i\beta \frac{\partial \phi}{\partial z} - \frac{\partial^2 \phi}{\partial z^2} = P\phi. \tag{2.85}$$

For each of the TE and TM mode, it is expressed as below.

$$\text{TE mode} : P = \frac{\partial^2 \phi}{\partial x^2} + k_0^2(\varepsilon_r - n_{eff}^2) \tag{2.86a}$$

$$\text{TM mode} : P = \varepsilon_r \frac{\partial}{\partial x}\left(\frac{1}{\varepsilon}\frac{\partial}{\partial x}\right) + k_0^2(\varepsilon_r - n_{eff}^2) \tag{2.86b}$$

Solving Eq. (2.85) formally, we get following.

$$\frac{\partial}{\partial z}\left(1+\frac{i}{2\beta}\frac{\partial}{\partial z}\right)\phi = -\frac{jP}{2\beta}\phi$$

$$\therefore \frac{\partial\phi}{\partial z} = \frac{-\frac{jP}{2\beta}}{1+\frac{j}{2\beta}\frac{\partial}{\partial z}}\phi \tag{2.87}$$

Omitting the differentiation of denominator of Eq. (2.87), it results Fresnel approximation.

$$\left.\frac{\partial}{\partial z}\right|_n = \frac{-\frac{jP}{2\beta}}{1+\frac{j}{2\beta}\left.\frac{\partial}{\partial z}\right|_{n-1}} \tag{2.88}$$

Consider the Eq. (2.87) as a recursive expression and replace the derivative of the right-hand side denominator by Eq. (2.88). Then, let's find definite expression in case of increased order of Eq. (2.88). First of all, define the start of the recursive expression.

$$\left.\frac{\partial}{\partial z}\right|_{-1} = 0 \tag{2.89}$$

Hereinafter, an expression corresponding to the order of the wide angle is obtained.

(1) WA-0th order (Fresnel approximation)

$$\left.\frac{\partial}{\partial z}\right|_0 = \frac{-\frac{jP}{2\beta}}{1+\frac{j}{2\beta}\left.\frac{\partial}{\partial z}\right|_{-1}} = -j\frac{P}{2\beta} \tag{2.90}$$

(2) WA-1st order

$$\left.\frac{\partial}{\partial z}\right|_1 = \frac{-\frac{jP}{2\beta}}{1+\frac{j}{2\beta}\left.\frac{\partial}{\partial z}\right|_0} = -j\frac{\frac{P}{2\beta}}{1+\frac{P}{4\beta^2}} \tag{2.91}$$

(3) WA-2nd order

$$\left.\frac{\partial}{\partial z}\right|_2 = \frac{-\frac{jP}{2\beta}}{1+\frac{j}{2\beta}\left.\frac{\partial}{\partial z}\right|_1} = -j\frac{\frac{P}{2\beta}+\frac{P^2}{8\beta^3}}{1+\frac{P}{2\beta^2}} \tag{2.92}$$

(4) WA-3rd order

$$\left.\frac{\partial}{\partial z}\right|_3 = \frac{-\frac{jP}{2\beta}}{1+\frac{j}{2\beta}\left.\frac{\partial}{\partial z}\right|_2} = -j\frac{\frac{P}{2\beta}+\frac{P^2}{4\beta^3}}{1+\frac{3P}{4\beta^2}+\frac{P^2}{16\beta^4}} \tag{2.93}$$

(5) WA-4th order

$$\left.\frac{\partial}{\partial z}\right|_4 = \frac{-\frac{jP}{2\beta}}{1+\frac{j}{2\beta}\left.\frac{\partial}{\partial z}\right|_3} = -j\frac{\frac{P}{2\beta}+\frac{3P^2}{8\beta^3}+\frac{P^3}{32\beta^3}}{1+\frac{P}{\beta^2}+\frac{3P^2}{16\beta^4}} \tag{2.94}$$

(6) WA-5th order

$$\left.\frac{\partial}{\partial z}\right|_5 = \frac{-\frac{jP}{2\beta}}{1+\frac{j}{2\beta}\left.\frac{\partial}{\partial z}\right|_4} = -j\frac{\frac{P}{2\beta}+\frac{P^2}{2\beta^3}+\frac{3P^3}{32\beta^5}}{1+\frac{5P}{4\beta^2}+\frac{3P^2}{8\beta^4}+\frac{P^3}{64\beta^6}} \tag{2.95}$$

(7) WA-6th order

$$\left.\frac{\partial}{\partial z}\right|_6 = \frac{-\frac{jP}{2\beta}}{1+\frac{j}{2\beta}\left.\frac{\partial}{\partial z}\right|_5} = -j\frac{\frac{P}{2\beta}+\frac{5P^2}{8\beta^3}+\frac{3P^3}{16\beta^5}+\frac{P^4}{128\beta^7}}{1+\frac{3P}{2\beta^2}+\frac{5P^2}{8\beta^4}+\frac{P^3}{16\beta^6}} \tag{2.96}$$

(8) WA-7th order

$$\left.\frac{\partial}{\partial z}\right|_7 = \frac{-\frac{jP}{2\beta}}{1+\frac{j}{2\beta}\left.\frac{\partial}{\partial z}\right|_6} = -j\frac{\frac{P}{2\beta}+\frac{3P^2}{4\beta^3}+\frac{5P^3}{16\beta^5}+\frac{P^4}{32\beta^7}}{1+\frac{7P}{4\beta^2}+\frac{15P^2}{16\beta^4}+\frac{5P^3}{32\beta^6}+\frac{P^4}{256\beta^8}} \tag{2.97}$$

Therefore, the recursive expression obtained by the Eq. (2.88) is a rational expression including only the operator P, and it can be understood that N of the numerator and D of the denominator are polynomials of the operator P.

$$\frac{\partial\phi}{\partial z} = -j\frac{N}{D}\phi \tag{2.98}$$

There is following relationship between the order of wide angle and the order of Padé approximation.

$WA-0 \leftrightarrow (1,0)$
$WA-1 \leftrightarrow (1,1)$
$WA-2 \leftrightarrow (2,1)$
$WA-3 \leftrightarrow (2,2)$
$WA-4 \leftrightarrow (3,2)$
$WA-5 \leftrightarrow (3,3)$
$WA-6 \leftrightarrow (4,3)$
$WA-7 \leftrightarrow (4,4)$

After that, for the Eq. (2.98), applying a incremental difference based on the crank-Nicholson method yields, following expression is obtained.

$$\left.\begin{array}{c} \frac{\partial\phi}{\partial z} \rightarrow \frac{1}{\triangle z}(\phi^{l+1}-\phi^l) \\ -j\frac{N}{D}\phi \rightarrow -j\frac{N}{D}\frac{1}{2}(\phi^{l+1}-\phi^l) \end{array}\right\} \tag{2.99}$$

In addition, on the right side, l and $l+1$ are averaged in order to match the difference center.

$$\frac{1}{\Delta z}(\phi^{l+1}-\phi^l) = -j\frac{N}{D}\frac{1}{2}(\phi^{l+1}+\phi^l)$$

$$\therefore D(\phi^{l+1}-\phi^l) = -jN\Delta z\frac{1}{2}(\phi^{l+1}+\phi^l)$$

$$\therefore (D+j\frac{\Delta z}{2}N)\phi^{l+1} = (D-j\frac{\Delta z}{2}N)\phi^l \tag{2.100}$$

From Eq. (2.99), we get

$$\therefore \phi^{l+1} = \frac{D-j\frac{\Delta z}{2}N}{D+j\frac{\Delta z}{2}N}\phi^l. \tag{2.101}$$

Since the coefficients in polynomials D and N in Eq. (2.98), it can be understood that D and N are also real numbers. Therefore, the following equation can be obtained.

$$\begin{aligned} \phi^{l+1} &= \frac{D - j\frac{\Delta z}{2}N}{(D + j\frac{\Delta z}{2}N)^*}\phi^l \\ &= \frac{\sum_{i=0}^{n} \xi_i P^i}{\sum_{i=0}^{n} \xi_i^* P^i}\phi^l \end{aligned} \tag{2.102}$$

Next, coefficients ξ_i are defined for the WA-0 to WA-7th order.
(1) WA-0th order: From Eq. (2.90)

$$\begin{aligned} D &= 1 \\ N &= \frac{P}{2\beta} \end{aligned}$$

$$\therefore D - j\frac{\Delta z}{2}N = 1 - j\frac{\Delta z}{2}\frac{P}{2\beta} \tag{2.103}$$

Therefore,

$$\left.\begin{aligned} \xi_0 &= 1 \\ \xi_1 &= -j\tfrac{\Delta z}{4\beta} \end{aligned}\right\} \tag{2.104}$$

(2) WA-1st order: From Eq. (2.91)

$$\begin{aligned} D &= 1 + \frac{P}{4\beta^2} \\ N &= \frac{P}{2\beta} \end{aligned}$$

$$\therefore D - j\frac{\Delta z}{2}N = 1 + \frac{1}{4\beta^2}(1 - j\beta z\Delta)P \tag{2.105}$$

Therefore,

$$\left.\begin{aligned} \xi_0 &= 1 \\ \xi_1 &= \tfrac{1}{4\beta^2}(1 - j\beta z\Delta)P \end{aligned}\right\} \tag{2.106}$$

(3) WA-2nd order: From Eq. (2.92)

$$\begin{aligned} D &= 1 + \frac{P}{2\beta^2} \\ N &= \frac{P}{2\beta} + \frac{P^2}{8\beta^3} \end{aligned}$$

$$\therefore D - j\frac{\Delta z}{2}N = 1 + \frac{1}{4\beta^2}(2 - j\beta z\Delta)P - j\frac{\Delta z}{16\beta^3}P^2 \tag{2.107}$$

Therefore,

$$\left.\begin{aligned} \xi_0 &= 1 \\ \xi_1 &= \tfrac{1}{4\beta^2}(2 - j\beta z\Delta) \\ \xi_2 &= -j\tfrac{\Delta z}{16\beta^3} \end{aligned}\right\} \tag{2.108}$$

(4) WA-3rd order: From Eq. (2.93)

$$\begin{aligned} D &= 1+\frac{3P}{4\beta^2}+\frac{P^2}{16\beta^4} \\ N &= \frac{P}{2\beta}+\frac{P^2}{4\beta^3} \end{aligned}$$

$$\therefore D-j\frac{\Delta z}{2}N = 1+\frac{1}{4\beta^2}(3-j\beta z\Delta)P+\frac{1}{16\beta^4}(1-j2\beta z\Delta)P^2 \tag{2.109}$$

Therefore,

$$\left.\begin{aligned} \xi_0 &= 1 \\ \xi_1 &= \tfrac{1}{4\beta^2}(3-j\beta z\Delta) \\ \xi_2 &= \tfrac{1}{16\beta^4}(1-j2\beta z\Delta) \end{aligned}\right\} \tag{2.110}$$

(5) WA-4th order: From Eq. (2.94)

$$\begin{aligned} D &= 1+\frac{P}{\beta^2}+\frac{3P^2}{16\beta^4} \\ N &= \frac{P}{2\beta}+\frac{3P^2}{8\beta^3}+\frac{P^3}{32\beta^5} \end{aligned}$$

$$\therefore D-j\frac{\Delta z}{2}N = 1+\frac{1}{4\beta^2}(4-j\beta z\Delta)P+\frac{1}{16\beta^4}(3-j3\beta z\Delta)P^2-j\frac{\Delta z}{64\beta^5}P^3 \tag{2.111}$$

Therefore,

$$\left.\begin{aligned} \xi_0 &= 1 \\ \xi_1 &= \tfrac{1}{4\beta^2}(4-j\beta z\Delta) \\ \xi_2 &= \tfrac{1}{16\beta^4}(3-j3\beta z\Delta) \\ \xi_3 &= -j\tfrac{\Delta z}{64\beta^5}P^3 \end{aligned}\right\} \tag{2.112}$$

(6) WA-5th order: From Eq. (2.95)

$$\begin{aligned} D &= 1+\frac{5P}{4\beta^2}+\frac{3P^2}{8\beta^4}+\frac{P^3}{64\beta^6} \\ N &= \frac{P}{2\beta}+\frac{P^2}{2\beta^3}+\frac{3P^3}{32\beta^5} \end{aligned}$$

$$\begin{aligned} \therefore D-j\frac{\Delta z}{2}N = \quad & 1 \quad +\frac{1}{4\beta^2}(5-j\beta z\Delta)P+\frac{1}{8\beta^4}(3-j2\beta z\Delta)P^2 \\ & + \quad \frac{1}{64\beta^6}(1-j3\beta z\Delta)P^3 \end{aligned} \tag{2.113}$$

Therefore,

$$\left.\begin{aligned} \xi_0 &= 1 \\ \xi_1 &= \tfrac{1}{4\beta^2}(5-j\beta z\Delta) \\ \xi_2 &= \tfrac{1}{8\beta^4}(3-j2\beta z\Delta) \\ \xi_3 &= \tfrac{1}{64\beta^6}(1-j3\beta z\Delta) \end{aligned}\right\} \tag{2.114}$$

(7) WA-6th order: From Eq. (2.96)

$$\begin{aligned} D &= 1+\frac{3P}{2\beta^2}+\frac{5P^2}{8\beta^4}+\frac{P^3}{16\beta^6} \\ N &= \frac{P}{2\beta}+\frac{P^2}{8\beta^3}+\frac{3P^3}{16\beta^5}+\frac{P^4}{128\beta^7} \end{aligned}$$

$$\begin{aligned} \therefore D-j\frac{\Delta z}{2}N = \quad & 1 \quad +\frac{1}{4\beta^2}(6-j\beta z\Delta)P+\frac{1}{16\beta^4}(10-j5\beta z\Delta)P^2 \\ & + \quad \frac{1}{32\beta^6}(2-j3\beta z\Delta)P^3-\frac{j\Delta z}{256\beta^7}P^4 \end{aligned} \tag{2.115}$$

Therefore,

$$\left.\begin{array}{rcl} \xi_0 &=& 1 \\ \xi_1 &=& \frac{1}{4\beta^2}(6-j\beta z\Delta) \\ \xi_2 &=& \frac{1}{16\beta^4}(10-j5\beta z\Delta) \\ \xi_3 &=& \frac{1}{32\beta^6}(2-j3\beta z\Delta) \\ \xi_4 &=& -\frac{j\Delta z}{256\beta^7} \end{array}\right\} \tag{2.116}$$

(8) WA-7th order: From Eq. (2.97)

$$\begin{aligned} D &= 1+\frac{7P}{4\beta^2}+\frac{15P^2}{16\beta^4}+\frac{5P^3}{32\beta^6}+\frac{P^4}{256\beta^8} \\ N &= \frac{P}{2\beta}+\frac{3P^2}{4\beta^3}+\frac{5P^3}{16\beta^5}+\frac{P^4}{128\beta^7} \end{aligned}$$

$$\begin{aligned} \therefore D-j\frac{\Delta z}{2}N = \quad & 1 \quad +\frac{1}{4\beta^2}(7-j\beta z\Delta)P+\frac{1}{16\beta^4}(15-j6\beta z\Delta)P^2 \\ & + \quad \frac{1}{32\beta^6}(5-j5\beta z\Delta)P^3+\frac{1}{256\beta^8}(1-j4\beta z\Delta)P^4 \end{aligned} \tag{2.117}$$

Therefore,

$$\left.\begin{array}{rcl} \xi_0 &=& 1 \\ \xi_1 &=& \frac{1}{4\beta^2}(7-j\beta z\Delta) \\ \xi_2 &=& \frac{1}{16\beta^4}(15-j6\beta z\Delta) \\ \xi_3 &=& \frac{1}{32\beta^6}(5-j5\beta z\Delta) \\ \xi_4 &=& \frac{1}{256\beta^8}(1-j4\beta z\Delta) \end{array}\right\} \tag{2.118}$$

As a result, $D-j(\Delta z/2)N$ was found. From them, $D+j(\Delta z/2)N$ can also be defined easily, so ϕ^{l+1} can be found from Eq. (2.100).

The simultaneous equations solved in the Eq. (2.84) became a triple diagonal form because the operator P containing the second order differential is included in the Fresnel approximation expression and the second order differentiation can be approximated by three terms. However, in the wide angle Eqs. (2.90) $\sim$ (2.97), operator P should be in higher order. Therefore, the Eq. (2.100) for these wide-angle equations is a simultaneous equation having

more coefficient matrix than three terms, and the Thomas method can not be applied. To solve this problem, we consider the multi-step method proposed by Hadley.

For Eq. (2.102), the numerator has already been determined by the above procedure, and the denominator can be obtained directly as the complex conjugate of the numerator. Since $\xi_0 = 1$ in these equations, it can be expressed as follows.

$$Numerator = \sum_{i=0}^{n} \xi_i P^i = (1 + a_n P) \cdots (1 + a_2 P)(1 + a_1 P) \tag{2.119}$$

The coefficients a_1, a_2, ..., a_n are obtained by solving the polynomials.

$$D - j\frac{\Delta z}{2} N = \sum_{i=0}^{n} \xi_i P^i = 0 \tag{2.120}$$

On the other hand, as can be seen from the denominator of Eq. (2.102), it can be found from the complex conjugate of the numerator coefficients a_1, a_2, ..., a_n.

$$\begin{aligned} Numerator &= \sum_{i=0}^{n} \xi_i^* P^i = (1 + a_n P)^* \cdots (1 + a_2 P)^* (1 + a_1 P)^* \\ &= (1 + a_n^* P) \cdots (1 + a_2^* P)(1 + a_1^* P) \end{aligned} \tag{2.121}$$

Therefore, the relationship of unknown wave function ϕ^{l+1} at the coordinate $z + \Delta z$ and the known wave function ϕ^l at the coordinate z is expressed by below.

$$\phi^{l+1} = \frac{(1 + a_n P) \cdots (1 + a_2 P)(1 + a_1 P)}{(1 + a_n^* P) \cdots (1 + a_2^* P)(1 + a_1^* P)} \phi^l \tag{2.122}$$

To solve Eq. (2.122) it will be modified as follow.

$$\frac{(1 + a_n^* P) \cdots (1 + a_2^* P)}{(1 + a_n P) \cdots (1 + a_2 P)} \phi^{l+1} = \frac{(1 + a_1 P)}{(1 + a_1^* P)} \phi^l \tag{2.123}$$

Here,

$$\phi^{l+\frac{1}{n}} = \frac{(1 + a_n^* P) \cdots (1 + a_2^* P)}{(1 + a_n P) \cdots (1 + a_2 P)} \phi^{l+1} \tag{2.124}$$

and Eq. (2.123) will be expressed as

$$\phi^{l+\frac{1}{n}} = \frac{(1 + a_1 P)}{(1 + a_1^* P)} \phi^l. \tag{2.125}$$

Since ϕ^l is known, $\phi^{l+\frac{1}{n}}$ is determined. Using $\phi^{l+\frac{1}{n}}$, Eq. (2.125) becomes

$$\frac{(1 + a_n^* P) \cdots (1 + a_3^* P)}{(1 + a_n P) \cdots (1 + a_3 P)} \phi^{l+1} = \frac{(1 + a_2 P)}{(1 + a_2^* P)} \phi^{l+\frac{1}{n}}. \tag{2.126}$$

If it is abbreviated as

$$\phi^{l+\frac{2}{n}} = \frac{(1 + a_n^* P) \cdots (1 + a_3^* P)}{(1 + a_n P) \cdots (1 + a_3 P)} \phi^{l+1} \tag{2.127}$$

$$\phi^{l+\frac{2}{n}} = \frac{(1+a_2 P)}{(1+a_2^* P)}\phi^{l+\frac{1}{n}} \tag{2.128}$$

and by solving it, $\phi^{l+\frac{2}{n}}$ is obtained. By repeating this procedure, the unknown wave function ϕ^{l+1} at coordinate $z+\Delta z$ can be found.

$$\phi^{l+1} = \frac{(1+a_n P)}{(1+a_n^* P)}\phi^{l+\frac{n-1}{n}} \tag{2.129}$$

On the other hand, unknown ϕ^{l+1} can be calculated from known ϕ^l by obtaining the following equation in order of $i = 1, 2, ..., n$.

$$\phi^{l+\frac{i}{n}} = \frac{(1+a_i P)}{(1+a_i^* P)}\phi^{l+\frac{i-1}{n}} \tag{2.130}$$

Chapter 3

Quality Parameters of Optical Network

During the signal transmission various kinds of optical effects cause distortion and degrade transmission quality. Among them a noise is main factor. In optical communication systems, an amplifier is commonly used to compensate signal loss. A light wave is generated by stimulated emission or spontaneous emission. An amplified spontaneous emission (ASE) is an amplification for spontaneous emitted light which has random phase and frequency, and it propagates in all directions. The ASE is considered as a main noise source for the amplifiers [17].

3.1 Optical signal-to-noise ratio (OSNR)

The noise is characterized as a term called signal-to-noise ratio (SNR) which can be defined as below in term of signal power.

$$SNR = \frac{mean\ signal\ power}{mean\ noise\ power} = \frac{S}{N} \tag{3.1}$$

In digital or data communication, since the information is referred as bits or symbols, the SNR is defined by energy or power per modulation symbol [19].

$$SNR = \frac{E}{N_0} = \frac{P}{N_0 R_s} \tag{3.2}$$

Here, N_0 is power spectral density and R_s is symbol rate. Besides it, SNR per bit is mostly used to compare modulation formats and defined as

$$SNR_b = \frac{SNR}{\widetilde{R}} \tag{3.3}$$

where, $\widetilde{R}$ is number of information bits per symbol.

In optical data communications a term called optical SNR (OSNR) is used.

$$OSNR = \frac{P}{2N_{ASE}B_{ref}} \tag{3.4}$$

Here, N_{ASE} is spectral density of amplified spontaneous emission and B_{ref} is reference bandwidth which is a usually taken as a 12.5 GHz.

The relation between OSNR and SNR is expressed by

$$OSNR = \frac{pR_s}{2B_{ref}} SNR \tag{3.5}$$

where, p expresses the polarization states of the signal and where N_{ASE} and N_0 are assumed to be equivalent.

In terms of SNR per bit, OSNR is expressed as

$$OSNR = \frac{R_b}{2B_{ref}} SNR_b \tag{3.6}$$

where, R_b is the information bit rate and defined by $R_b = p\widetilde{R}R_s$.

In decibels,

$$OSNR(dB) = 10log_{10}OSNR. \tag{3.7}$$

A presence of noise in communications causes bit error and it is defined as bit-error rate (BER) term expressed by below equation.

$$BER = \lim_{N \to \infty} \frac{N_e}{N} \tag{3.8}$$

Here, N_e is number of incorrectly received bits and N is number of transmitted bits. Depending on SNR, BER can be defined as

$$BER = \frac{1}{2} erfc(\sqrt{\frac{E}{N_0}}) = \frac{1}{2} erfc(\sqrt{SNR}). \tag{3.9}$$

A BER curve as a function of SNR or OSNR is mostly used to describe performance of digital communication system.

Chapter 4

Basis of Proposed Method

So far, our research group has proposed waveguide-type circuits for recognition of BPSK, QPSK, 16 QAM coded labels as mentioned before. In this work, we design 8QAM coded label recognition circuit based on former QPSK code recognition circuit (QPRC) [11] with proper adjustments.

4.1 Waveguide elements of QPRC

To built up QPRC, several types of waveguide elements including 3-dB couplers, Y-junctions, and asymmetric X-junctions are assembled together. Figure 4.1 shows structure of each elements, respectively.

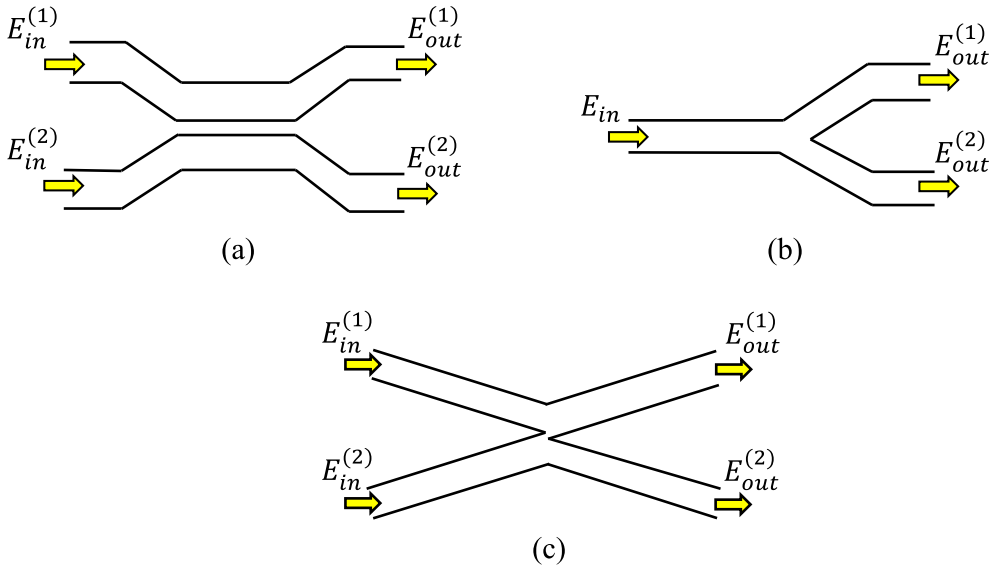

Figure 4.1: Waveguide elements of QPRC, (a) 3-dB coupler, (b) Y-junction, and (c) Asymmetric X-junction.

4.1.1 3-dB coupler

As shown in Figure 4.1 (a), 3-dB coupler consists of parallel single mode waveguides. It is used to split power equally into its two output ports. For 3-dB coupler, its outputs are 90 degrees out of phase with each other. The relation of input signals ($E_{in}^{(1)}$ and $E_{in}^{(2)}$) and output signals ($E_{out}^{(1)}$ and $E_{out}^{(2)}$) can be written as

$$\begin{pmatrix} E_{out}^{(1)} \\ E_{out}^{(2)} \end{pmatrix} = \frac{1}{\sqrt{2}} \begin{pmatrix} 1 & -j \\ -j & 1 \end{pmatrix} \begin{pmatrix} E_{in}^{(1)} \\ E_{in}^{(2)} \end{pmatrix} \tag{4.1}$$

where $j = \sqrt{-1}$.

4.1.2 Y-junction

Y-junction combines two single mode waveguides to one single mode waveguide at small angle as shown in Figure 4.1 (b). It is used to branch input light pulse equally into output ports and expressed as below.

$$\begin{pmatrix} E_{out}^{(1)} \\ E_{out}^{(2)} \end{pmatrix} = \frac{1}{\sqrt{2}} \begin{pmatrix} 1 \\ 1 \end{pmatrix} E_{in} \tag{4.2}$$

4.1.3 Asymmetric X-junction

An asymmetric X-junction coupler as illustrated in Figure 4.1 (c) can be designed as a combination of two Y-junctions. An Y-junction in the input consists of single mode waveguides with same widths while the output part has waveguides with different widths. A coupling characteristic of asymmetric X-coupler depends on the phase of input signals. If input signals are in phase, the output is obtained at the wider waveguide and vice versa. The following expression shows the input and output signals relation.

$$\begin{pmatrix} E_{out}^{(1)} \\ E_{out}^{(2)} \end{pmatrix} = \frac{1}{\sqrt{2}} \begin{pmatrix} 1 & 1 \\ -1 & 1 \end{pmatrix} \begin{pmatrix} E_{in}^{(1)} \\ E_{in}^{(2)} \end{pmatrix} \tag{4.3}$$

4.2 QPSK code recognition circuit (QPRC)

As explained in Section 1.1.2, QPSK code consists of four different phase values. Therefore, QPRC is designed to identify these phases. As shown in Figure 4.2, it consists of 3-dB coupler, asymmetric X-junction, and two Y-junctions. It has two input ports and four output ports which is dedicated to identify each of the phase values. The QPSK signal is given into one of the input port and a signal called reference signal is given into another one. An interference effect between QPSK and reference signals along the waveguide circuit results a unique output intensities corresponding to each of the phase value.

A relation between inputs and outputs are found as Eq. (4.4) and Eq. (4.5) by combining coupling characteristics of each waveguide element.

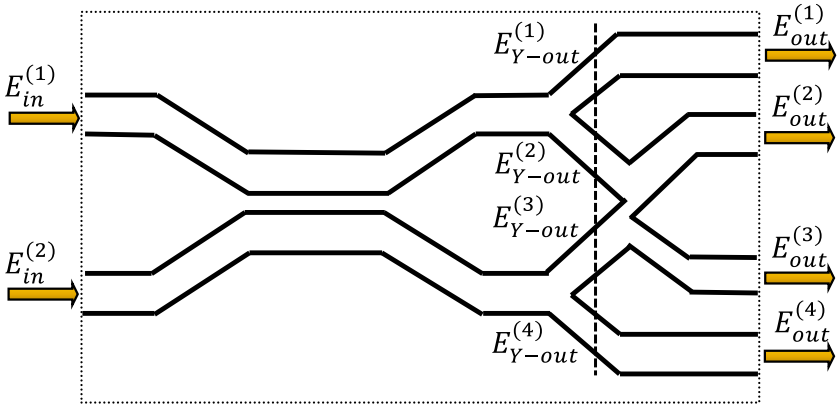

Figure 4.2: Structure of QPRC.

At the output of two Y-junctions, electric fields of the output signals are defined as below.

$$\begin{pmatrix} E_{Y-out}^{(1)} \\ E_{Y-out}^{(2)} \\ E_{Y-out}^{(3)} \\ E_{Y-out}^{(4)} \end{pmatrix} = \frac{1}{2} \begin{pmatrix} 1 & 0 \\ 1 & 0 \\ 0 & 1 \\ 0 & 1 \end{pmatrix} \begin{pmatrix} 1 & -j \\ -j & 1 \end{pmatrix} \begin{pmatrix} E_{in}^{(1)} \\ E_{in}^{(2)} \end{pmatrix} \tag{4.4}$$

After passing the asymmetric X-junction, the outputs of the QPRC are found as below expression.

$$\begin{pmatrix} E_{out}^{(1)} \\ E_{out}^{(2)} \\ E_{out}^{(3)} \\ E_{out}^{(4)} \end{pmatrix} = \frac{1}{2} \begin{pmatrix} 1 & 0 & 0 & 0 \\ 0 & \frac{1}{\sqrt{2}} & \frac{1}{\sqrt{2}} & 0 \\ 0 & -\frac{1}{\sqrt{2}} & \frac{1}{\sqrt{2}} & 0 \\ 0 & 0 & 0 & 1 \end{pmatrix} \begin{pmatrix} E_{Y-out}^{(1)} \\ E_{Y-out}^{(2)} \\ E_{Y-out}^{(3)} \\ E_{Y-out}^{(4)} \end{pmatrix}$$

$$= \frac{1}{2} \begin{pmatrix} 1 & -j \\ \frac{1-j}{\sqrt{2}} & \frac{1-j}{\sqrt{2}} \\ \frac{-1-j}{\sqrt{2}} & \frac{1+j}{\sqrt{2}} \\ -j & 1 \end{pmatrix} \begin{pmatrix} E_{in}^{(1)} \\ E_{in}^{(2)} \end{pmatrix} = \frac{1}{2} \begin{pmatrix} 1 & e^{j3\pi/2} \\ e^{j7\pi/4} & e^{j7\pi/4} \\ e^{j5\pi/4} & e^{j\pi/4} \\ e^{j\pi/2} & 1 \end{pmatrix} \begin{pmatrix} E_{in}^{(1)} \\ E_{in}^{(2)} \end{pmatrix} \tag{4.5}$$

Here, $E_{in}^{(1)}$ is reference signal and given as

$$E_{in}^{(1)} = 1 \tag{4.6}$$

and $E_{in}^{(2)}$ is QPSK signal with four different phases defined as below.

$$E_{in}^{(2)} = 1, j, -1, -j \tag{4.7}$$

Phase values in Eq. (4.7) are 0, $\frac{\pi}{2}$, π and $\frac{3\pi}{2}$, respectively.

By applying these input signal values into Eq. (4.5) we can obtain output intensities as shown in Table 4.1.

From output electric fields, output intensities can be found as shown in Table 4.2. From here, it can be seen that there are different minimum and maximum intensities are found for each input phase value. Therefore, with the aid of these unique intensities, phase values of QPSK signal can be identified through QPRC.

Table 4.1: Output electric fields of QPRC

Input	**Output**			
	$E_{out}^{(1)}$	$E_{out}^{(2)}$	$E_{out}^{(3)}$	$E_{out}^{(4)}$
$(E_{in}^{(1)},E_{in}^{(2)})=(1,1)$	$\frac{1}{\sqrt{2}}\ e^{j\pi/4}$	$e^{j5\pi/4}$	0	$\frac{1}{\sqrt{2}}\ e^{j5\pi/4}$
$(E_{in}^{(1)},E_{in}^{(2)})=(1,-1)$	$\frac{1}{\sqrt{2}}\ e^{j7\pi/4}$	0	$e^{j7\pi/4}$	$\frac{1}{\sqrt{2}}\ e^{j7\pi/4}$
$(E_{in}^{(1)},E_{in}^{(2)})=(1,j)$	1	$\frac{1}{\sqrt{2}}$	$-\frac{1}{\sqrt{2}}$	0
$(E_{in}^{(1)},E_{in}^{(2)})=(1,-j)$	0	$-\frac{1}{\sqrt{2}}$	$-\frac{1}{\sqrt{2}}$	$-j$

Table 4.2: Opical output intensities of QPRC

Input	**Output**			
	$\lvert E_{out}^{(1)}\rvert^2$	$\lvert E_{out}^{(2)}\rvert^2$	$\lvert E_{out}^{(3)}\rvert^2$	$\lvert E_{out}^{(4)}\rvert^2$
$(E_{in}^{(1)},E_{in}^{(2)})=(1,1)$	0.5	1	0	0.5
$(E_{in}^{(1)},E_{in}^{(2)})=(1,-1)$	0.5	0	1	0.5
$(E_{in}^{(1)},E_{in}^{(2)})=(1,j)$	1	0.5	0.5	0
$(E_{in}^{(1)},E_{in}^{(2)})=(1,-j)$	0	0.5	0.5	1

Chapter 5

Waveguide-Type Optical Circuits for Recognition of Optical 8QAM Coded Label

In this chapter, we discuss the proposal of 8QAM coded label recognition circuit [18]. The operation is theoretically analyzed and numerically simulated by FD-BPM.

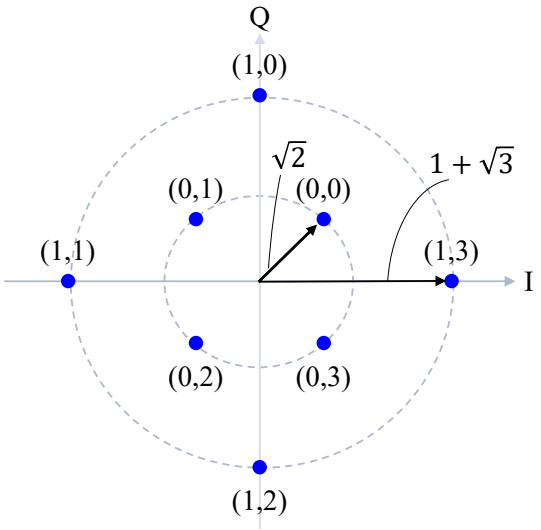

Figure 5.1: Constellation diagram of 8QAM signal.

5.1 8QAM coded signal

As stated briefly in Section 1.1.2, 8QAM signal has two amplitude values which has four different phase values respectively. Figure 5.1 depicts a constellation of 8QAM signal with its corresponding amplitude values and it can be expressed as

$$E_{8QAM} = a^m E_0 e^{j\pi/4} e^{jn\pi/2} e^{jm\pi/4} \tag{5.1}$$

where m=0, 1, n=0, 1, 2, 3, a=$(1+\sqrt{3})/\sqrt{2}$, and $a^m E_0$ defines an amplitude of 8QAM codes. The values on constellation points in constellation diagram relate to the combinations

of (m, n) and give different phase values.

It can be seen from Figure 5.1 that each of the amplitude values with four different phases can be treated like a QPSK code. Therefore we propose a 8QAM recognition circuit by using two QPSK code recognition circuits with corresponding adjustments.

5.2 Proposed recognition circuits

5.2.1 Minimum output recognition circuit for 1-symbol 8QAM code

A structure of proposed recognition circuit for 8QAM coded label is illustrated in Figure 5.2. It consists of two Y-junctions, a phase shifter, an attenuator and two QPRCs. With the aid of two Y-junctions at input, 8QAM and reference signals can be given to each of the inputs of QPRCs.

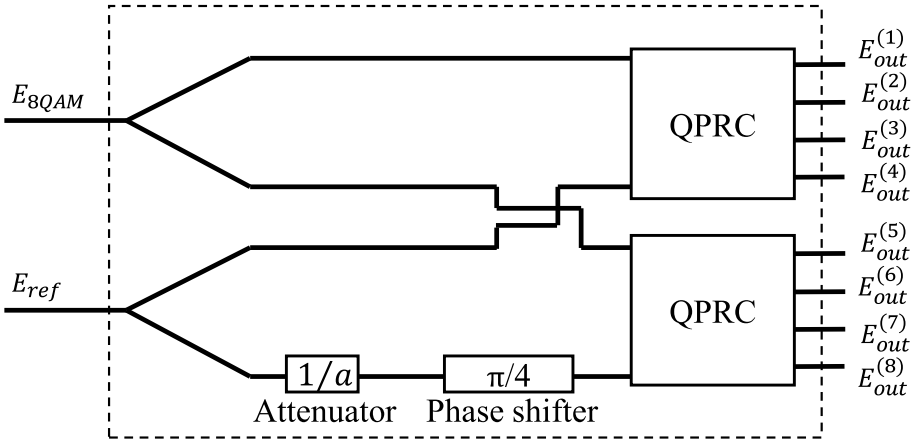

Figure 5.2: 8QAM coded label recognition circuit

A reference signal is assumed to be

$$E_{ref=}aE_0 \tag{5.2}$$

and it is attenuated by $\frac{1}{2}$ and phase shifted by $\frac{\pi}{4}$ to identify all of the amplitude and phase values at one of the inputs of one of the QPRCs.

Input-output relation of the 8QAM code recognition circuit (8QAM RC) can be defined as

$$\begin{pmatrix} E_{out}^{(1)} \\ \cdot \\ \cdot \\ E_{out}^{(8)} \end{pmatrix} = A_{8QAM} \begin{pmatrix} E_{8QAM} \\ E_{ref} \end{pmatrix} \tag{5.3}$$

where

$$A_{8QAM} = \frac{1}{2\sqrt{2}} \begin{pmatrix} 1 & e^{j3\pi/2} \\ e^{j7\pi/4} & e^{j7\pi/4} \\ e^{j5\pi/4} & e^{j\pi/4} \\ e^{j3\pi/2} & 1 \\ 1 & e^{j7\pi/4}/a \\ e^{j7\pi/4} & e^{j2\pi}/a \\ e^{j5\pi/4} & e^{j\pi/2}/a \\ e^{j3\pi/2} & e^{j\pi/4}/a \end{pmatrix}. \tag{5.4}$$

Theoretical analysis

In order to know the possibility of 8QAM code recognition with our proposed circuit, its operation is theoretically analyzed firstly. In this calculation, we assume that $E_0 = 1$. By applying it into Eq. (5.3) output intensities are found as shown in Figure 5.3 where $0.0005E_0^2$ is added into all of them as a crosstalk.

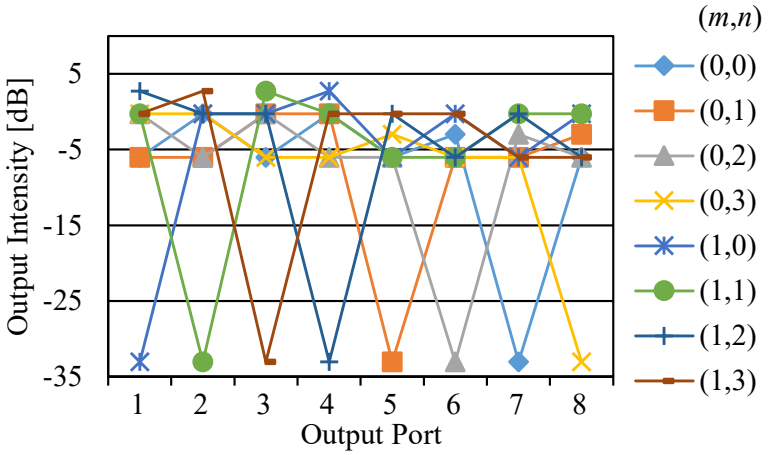

Figure 5.3: Theoretical results of output intensities for 8QAM RC

It can be understood that there are different null intensities found at output ports for each of the 8QAM code values. Therefore, the proposed recognition circuit can recognize 8QAM coded label as its minimum output ports. To discriminate null intensities from others, a post processing with thresholding device is expected to be used.

FD-BPM simulation

To verify theoretical calculation, a numerical simulation by FD-BPM is performed. A two-dimensional slab waveguide model is designed as illustrated in Figure 5.4. In simulation, two separate inputs, I_{2A} and I_{2B}, are used for reference signals to simplify the simulation by replacing the attenuator and the phase shifter. The 8QAM-coded signal is incident at I_1 input. For adjustment of the optical path lengths, several curved waveguides are used between the connections of the input waveguides to QPRCs.

Both of the E_{8QAM} and E_{ref} signals are supposed to be propagating at transverse electric (TE) mode at 1550-nm wavelength. The circuit is a silica-based waveguide with refractive

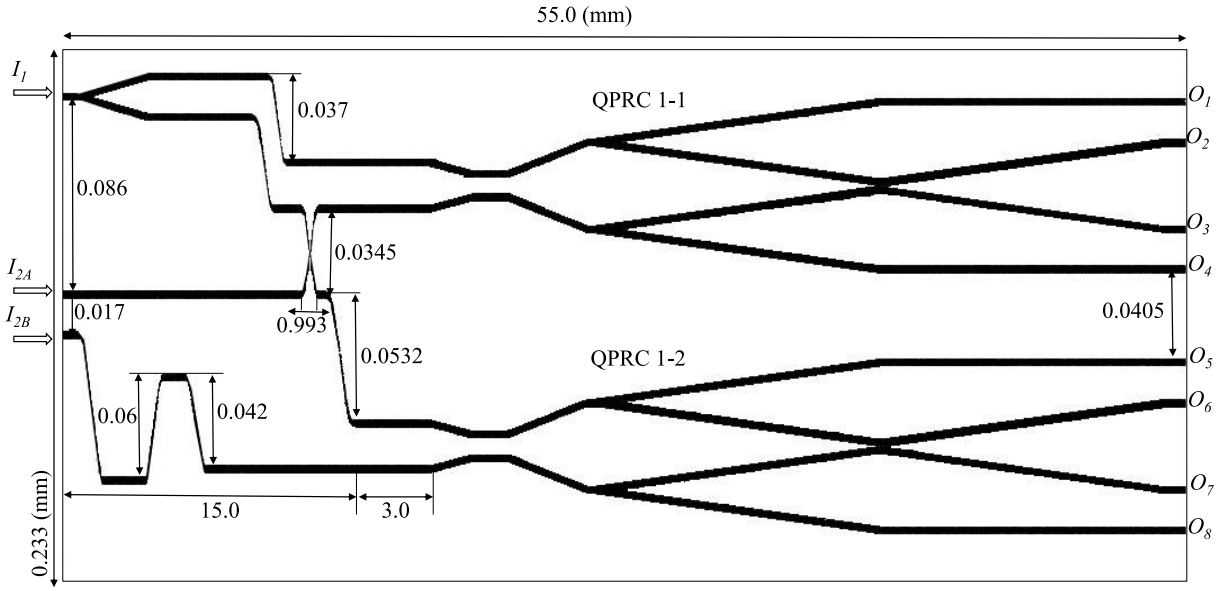

Figure 5.4: Two-dimensional slab waveguide model for 8QAM RC

indices 1.461 and 1.45 for core and cladding, respectively. The main width of the waveguide circuit W_0 is $3.0\mu m$. The total length of the waveguide circuit for 8QAM-coded label recognition circuit is 55 mm. A dimension details of QPRC is stated in Figure 5.5. For an asymmetric X-junction coupler, widths of the wide and narrow arms are designed as $W_w = 3.4\mu m$ and $W_n = 2.6\mu m$, respectively, with branch angle $\theta = 0.004rad$. The coupling region of the 3-dB coupler is L_c =1.734 mm with the gap of $d = 10.2\mu m$.

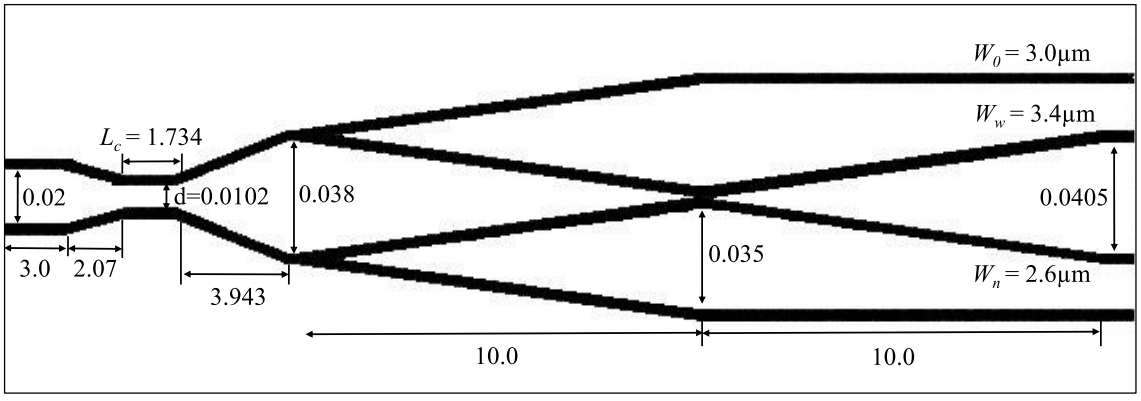

Figure 5.5: FD-BPM simulation model for QPRC

Optical intensities for $(m, n) = (0, 0)$ and $(m, n) = (1, 0)$ in logarithmic scale are illustrated in Figure 5.6 where the null intensities are clearly seen. The boundary between core and cladding region of the waveguide is overlaid by pale-colored lines for easy observation. The simulated optical intensities for all of the 8QAM codes are plotted in Figure 5.7 where null intensities are clearly clarified.

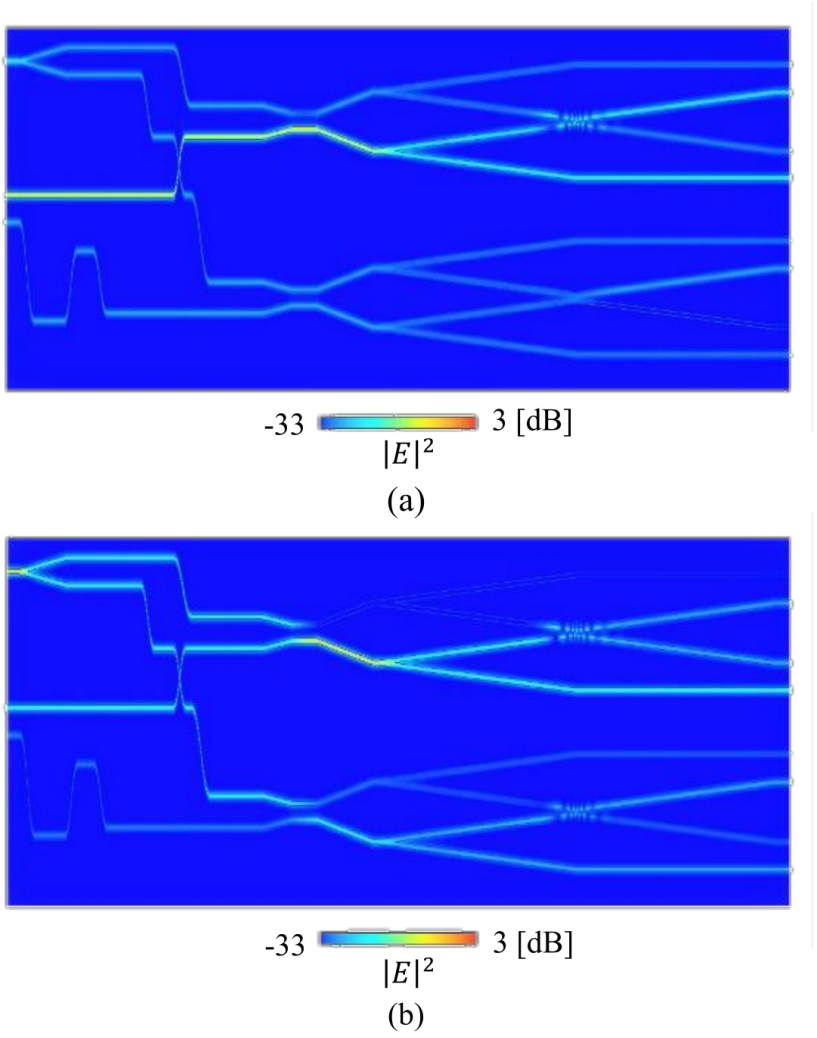

Figure 5.6: Simulated optical intensities along the circuit for (a) $(m, n) = (0, 0)$ and (b) $(m, n) = (1, 0)$

5.2.2 Minimum output recognition circuit for 2-symbol 8QAM code

In practical application, number of required labels is enormous. It was reported that a thousand to tens thousands of labels are required [19]. Therefore, we examine scalability of our proposed recognition method for 2-symbol length 8QAM coded label.

A scaled recognition circuit for 2-symbol length 8QAM coded label consists of two-stage connection of 8QAM RCs as shown in Figure 7.1. The first and the second 8QAM symbols are successively recognized by the first and the second stage, respectively.

Input-output relation for scaled circuit is expressed as Eq. (5.5) where $k = 1 \sim 8$. $E^{(2)}_{8QAM}$, E_{ref}, and A_{8QAM} are expressed by Eq. (5.1), Eq. (5.2), Eq. (5.3), and Eq. (5.4), respectively.

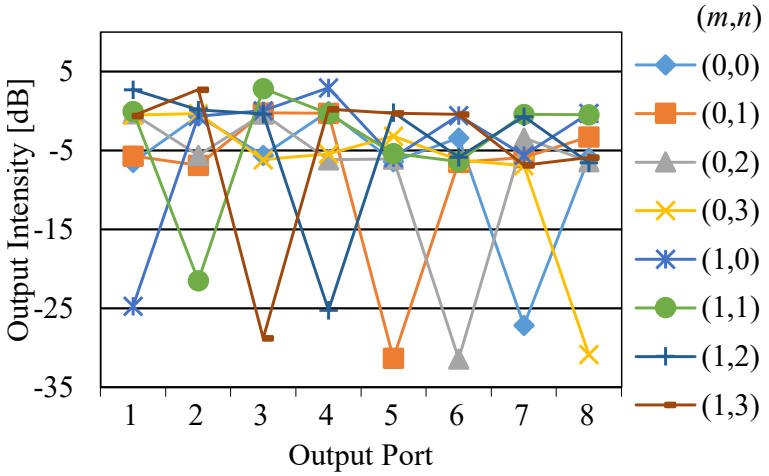

Figure 5.7: Simulated output intensities for all codes

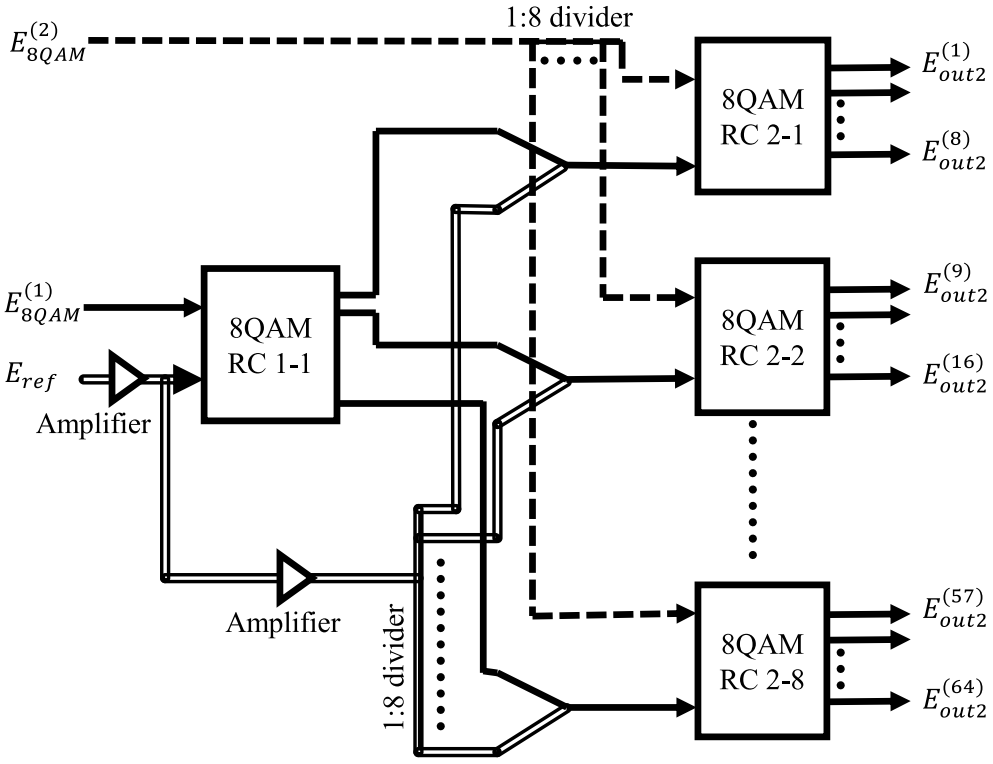

Figure 5.8: 2-symbol length 8QAM coded label recognition circuit

$$\begin{pmatrix} E_{out2}^{(1+8(k-1))} \\ \cdot \\ \cdot \\ E_{out2}^{(8+8(k-1))} \end{pmatrix} = A_{8QAM} \begin{pmatrix} \frac{E_{8QAM}^{(2)}}{\sqrt{8}} \\ \frac{E_{out1}^{(k)}}{\sqrt{2}} + \frac{E_{ref}}{\sqrt{8}} \end{pmatrix} \tag{5.5}$$

As an example, some of the output intensities found by theoretical calculation are illustrated in Figure 5.9 where (m, n) values are different for 1st symbol ($E_{8QAM}^{(1)}$) as listed in the legend and fixed (0,0) for 2nd symbol ($E_{8QAM}^{(2)}$). In this case, $0.0005E_0^2$ is added simi-

larly with 1-symbol length calculation. The maximum and the second minimum intensities are found as $0.458E_0^2$ and $0.001E_0^2$, respectively. For scaled recognition, a required dynamic range for post processing is found to be around 28 dB.

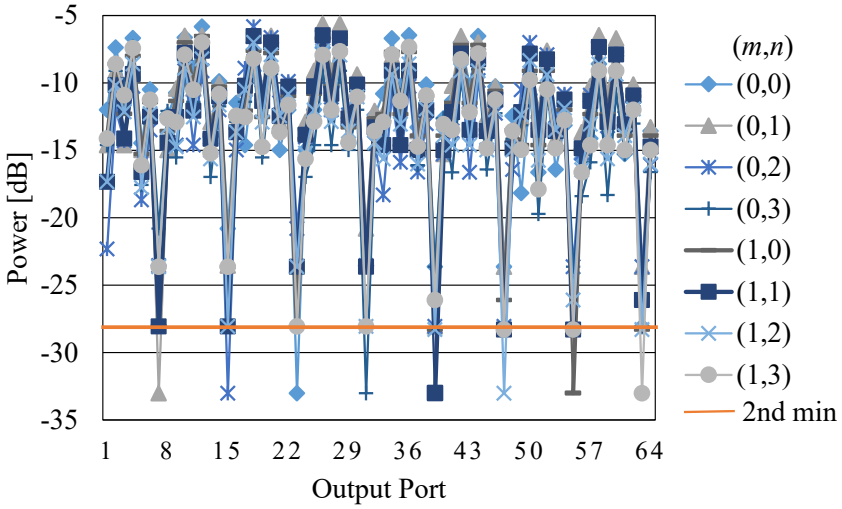

Figure 5.9: Output intensities for 2 symbol 8QAM code recognition in different (m, n) values for 1st symbol ($E_{8QAM}^{(1)}$) as listed in the legend and fixed (0,0) for 2nd symbol ($E_{8QAM}^{(2)}$)

5.2.3 Maximum output recognition circuit for 1-symbol 8QAM code

As the theoretical result in Fig. 5.7 shows, 8QAM code can not discriminated by maximum or non-null intensities directly with main proposed circuit. Therefore, we consider to use thresholding devices with logical circuits additionally as a post-processing. The thresholders with two different values, α and β, are connected to the output of main 8QAM recognition circuit as shown in Fig. 5.10 (a).

The structure of logical circuit is shown in Fig. 5.10 (b). The outputs of QPRCs ($E_{out1}^{(i)}$) found by Eq. (5.3) are thresholded by $\alpha = 1.4E_0^2$ and $\beta = 0.375E_0^2$ devices and then fed into the corresponding inputs of logical circuit as ordered. The final obtained result after logical circuit is shown in Fig. 5.11 where different outputs are found for each code.

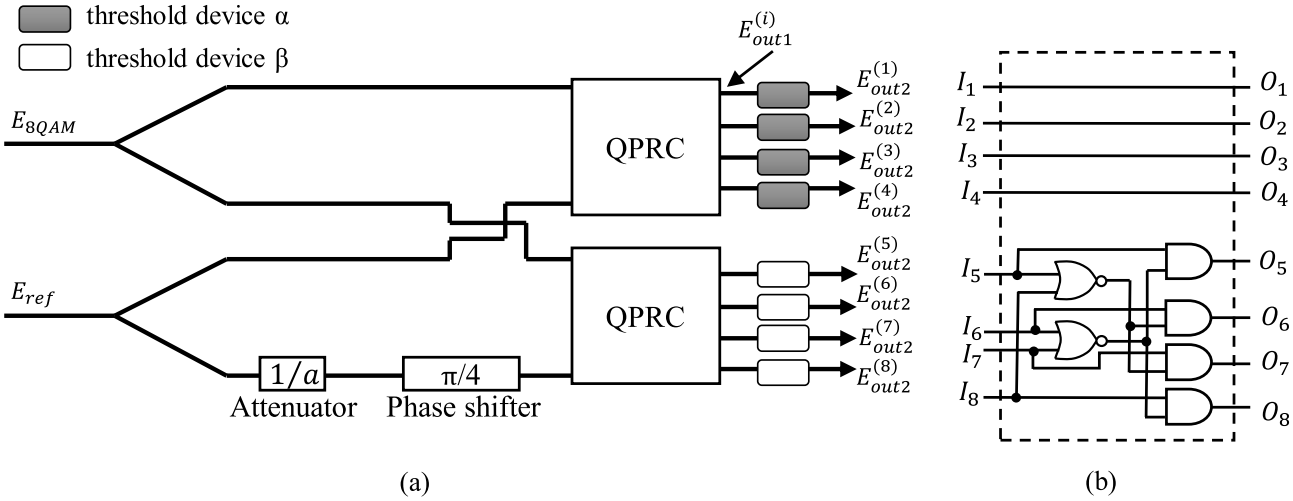

Figure 5.10: (a) Maximum output recognition circuit for 1-symbol 8QAM code, (b) Logical circuit

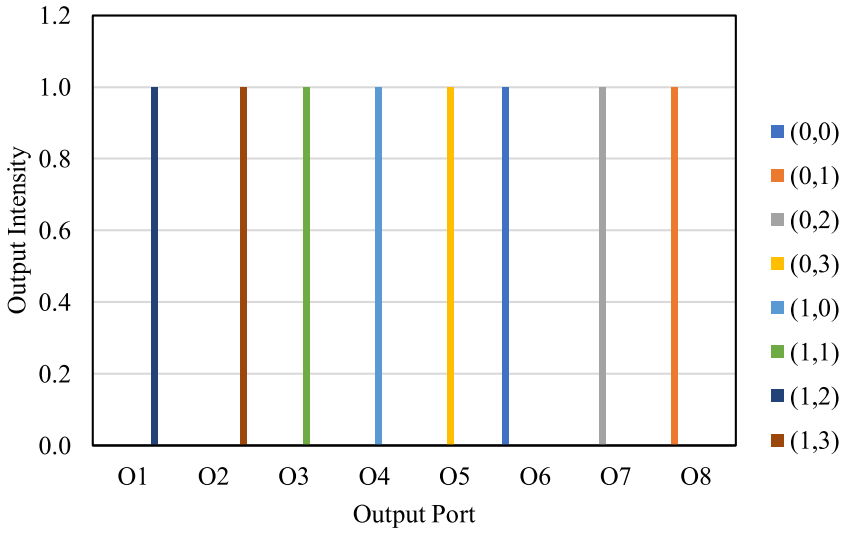

Figure 5.11: Output intensities after post processing logical circuit

Chapter 6

Evaluation of Noise Tolerance

As explained in Chapter 3, quality characteristics of communication network is an important factor. Therefore, in this chapter we discuss a noise tolerance evaluation for our proposed 8QAM label recognition circuits as a function of bit-error rate (BER) against optical signal-to-noise ratio (OSNR).

6.1 Evaluation of Noise Tolerance for 1-symbol 8QAM code recognition circuits

A designed simulation model at OptiSystem (Optiwave Systems Inc.) software is illustrated in Figure 6.1.

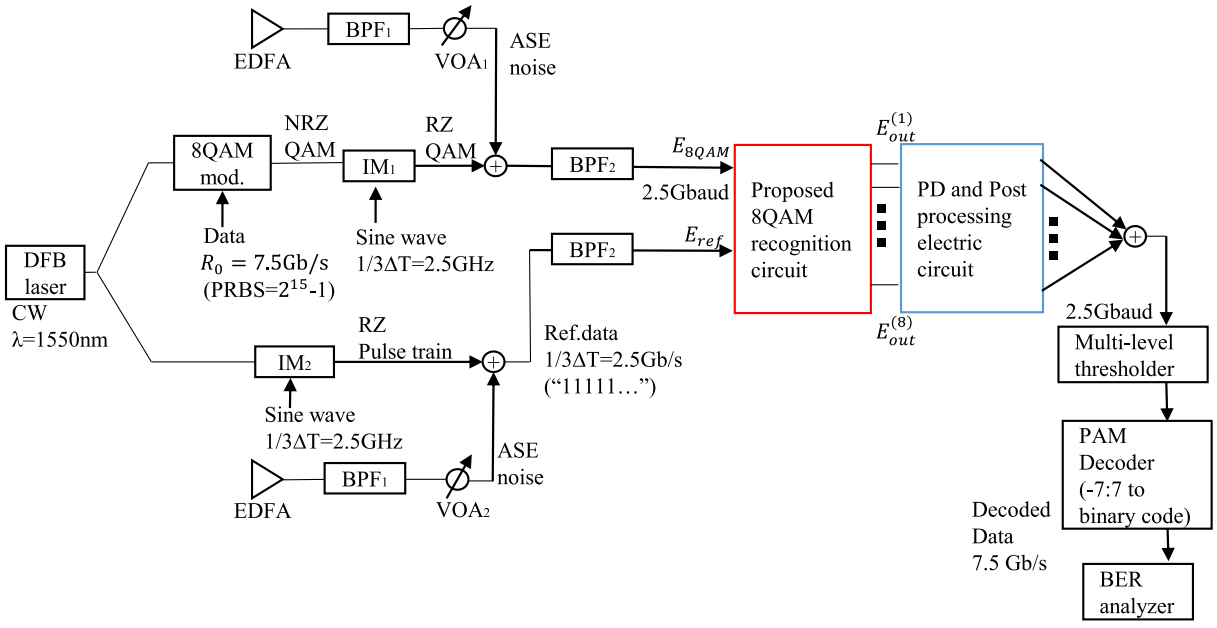

Figure 6.1: A simulation setup for one symbol 8QAM code recognition circuit.

Both of the 8QAM and reference signals are given from continuous wave (CW) laser source at wavelength of 1550 nm. The optical nonreturn-to-zero (NRZ) 8QAM pulse sequence at bit rate of R_0 = 7.5 Gb/s with symbol rate of $R_0/3$ = 2.5 Gbaud is generated

using pseudo random bit sequence of $2^{15} - 1$. To generate a return-to-zero (RZ) pulse sequence, the NRZ pulse sequence is modulated by sinusoidal wave at $R_0/3 = 2.5$ GHz. The reference signal is converted from NRZ to RZ pulse train in the similar manner. To generate optical 8QAM coded signal, we consider 8QAM modulator which consists of two intensity modulators (IM), a $\pi/2$ phase shifter, an optical power divider and a combiner. To evaluate noise tolerance, it is considered that amplified spontaneous emission (ASE) noise, which is generated from Er-ion doped fiber amplifier and band pass filtered by BPF_1 with 50 GHz bandwidth, is added to both of the signals. To adjust the noise level, variable optical attenuators (VOA_1 and VOA_2) are used. A BPF_2 with 5 GHz bandwidth is used to filter additional noise outside of the signal bandwidth.

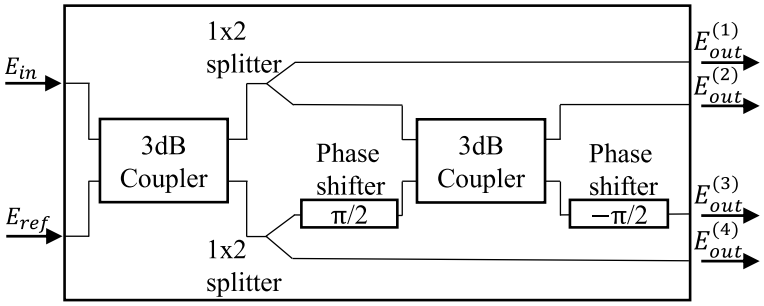

Figure 6.2: Equivalent simulation circuit model for QPRC

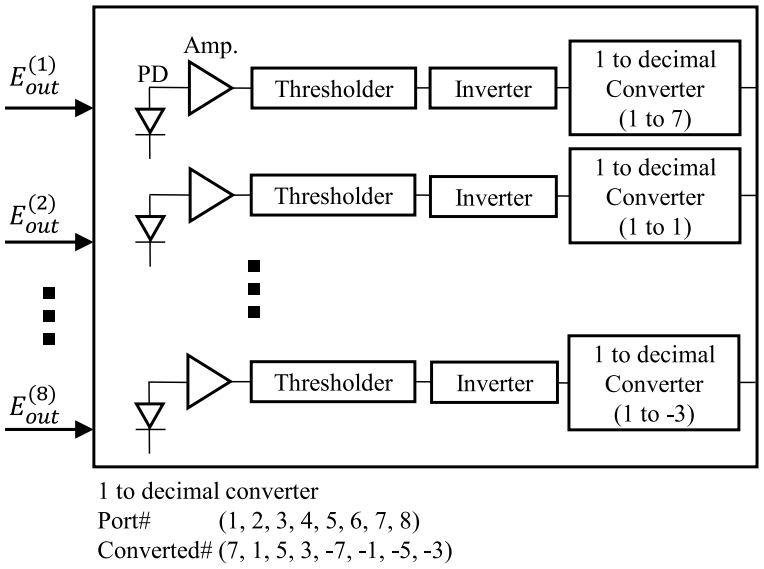

Figure 6.3: Post processing electric circuit

In this simulation, optical discrete devices are used to represent the waveguide recognition circuit. A structure of equivalent model for QPRC is shown in Figure 6.2 as designed previously [20], where the asymmetric X-junction coupler is represented by $\pi/2$ and $-\pi/2$ phase shifters and a 3-dB coupler. The 8QAM RC can be built with this equivalent QPRCs and other discrete devices.

To discriminate null output intensities, we consider to use a post processing circuit containing photodetectors (PDs), amplifiers, thresholders, inverters and 1 to decimal converters

as illustrated in Figure 6.3. After signal is detected with PDs, it is amplified by 60 dB. The thresholder converts the signal into 1 or 0 depending on whether the signal is higher or lower than its thresholding level. For the minimum recognition circuit, an optimal thresholding value should be lower than the second minimum intensity which is found around 0.78 mW in the simulation. We set the thresholding value at 0.3mW which is obtained as an optimal value as a result of measurements. For maximum output recognition circuit two different values, 4.5mW and 1.1mW, are set for α and β threshold devices.

After the thresholding process, the inverter is used to reverse the signal values by setting the null intensities into unitary signals and vice versa. The 1 to decimal converters are used to discriminate port numbers by converting the signals at each port into the corresponding values in Figure 6.3. The outputs of post processing circuit ranging from -7 to 7 are added with 8x1 combiner and are amplified. A multi-level thresholder and pulse amplitude modulation (PAM) decoder in Figure 6.1 are only used to retrieve 8QAM signal for BER analyzing process and are not required for label recognition function.

Examples of simulated signals at different points are illustrated in Figure 6.4. These signals are the 8QAM signal generated from binary data sequence, the reference signal, the optical output signal from port 1 of the recognition circuit, electric output signal from port 1 of the post processing circuit, and the multilevel output signal from multilevel thresholder from 8x1 combiner.

According to normalized constellation plots of the 8QAM codes at the entrance of the recognition circuit shown in Fig.6.5, added ASE noise induces amplitude and phase deviation. Two different OSNR values, 14 dB and 28 dB, are used here to capture constellation values.

The simulated BER performance as a function of OSNR at the entrance of both of the maximum and minimum 8QAM recognition circuits are plotted in Fig. 6.6. The BER performances are measured at symbol rates of 2.5-, 5- and 10-Gbaud. The required OSNRs for BER below $1.0\text{x}10^{-3}$ are around 7.8 dB, 10.8 dB and 13.9 dB for minimum recognition circuit and 11.6 dB, 14.6 dB and 17.7 dB for maximum recognition circuit. When the symbol rate doubles, the OSNR penalty was around 3dB. Compared with back-to-back (B2B) result, the OSNR penalties are around 1 dB and 5 dB for minimum and maximum recognition circuits at 2.5-Gbaud symbol rate, respectively. As the result shows, minimum recognition circuit tolerates more noise than maximum case due to the straightforward post processing scheme.

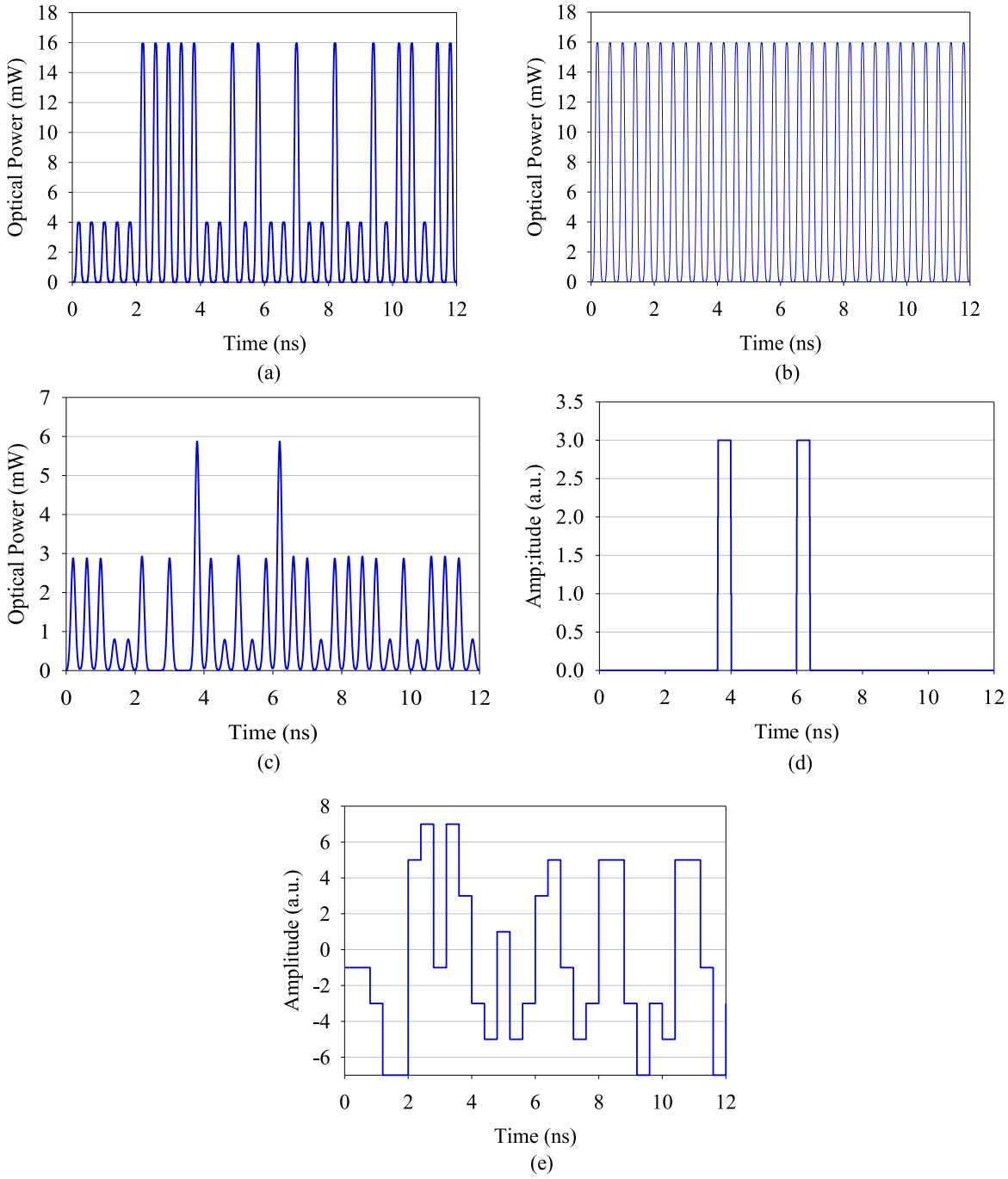

Figure 6.4: Examples of simulation signals (a) incident 8QAM signal, (b) reference signal, (c) optical output signal from port 1 of the recognition circuit, (d) electric output signal from port 1 of the post processing circuit, and (e) output signal from multilevel thresholder

6.2 Evaluation of Noise Tolerance for scaled 2-symbol recognition circuit

Noise tolerance for our scaled 2-symbol length recognition circuit is evaluated. A simulation set-up is illustrated in Figure 6.7 and it is configured in similar manner with 1-symbol

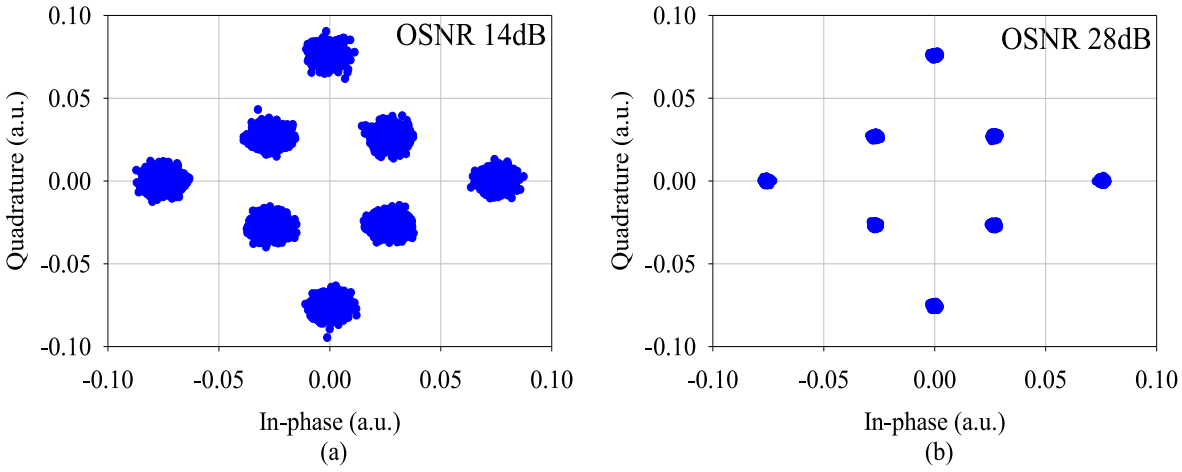

Figure 6.5: Noise added constellation plots; (a) OSNR=14 dB, (b) OSNR=28 dB

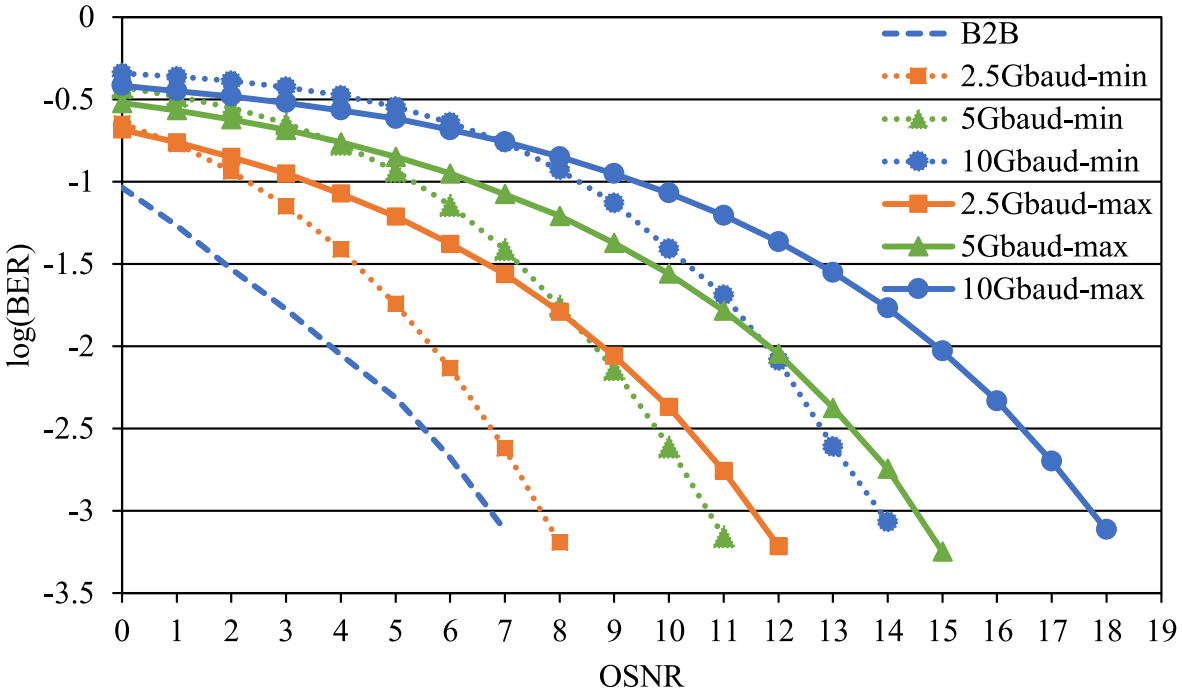

Figure 6.6: BER performance for 1-symbol 8QAM recognition circuits

simulation model.

A simulation is run for 2.5 Gbaud symbol rate and OSNR at BER of $1.0\text{x}10^{-3}$ is found around 20.8 dB. Compared with 1-symbol minimum recognition circuit result the BER penalty is around 13 dB as plotted in Figure 6.8.

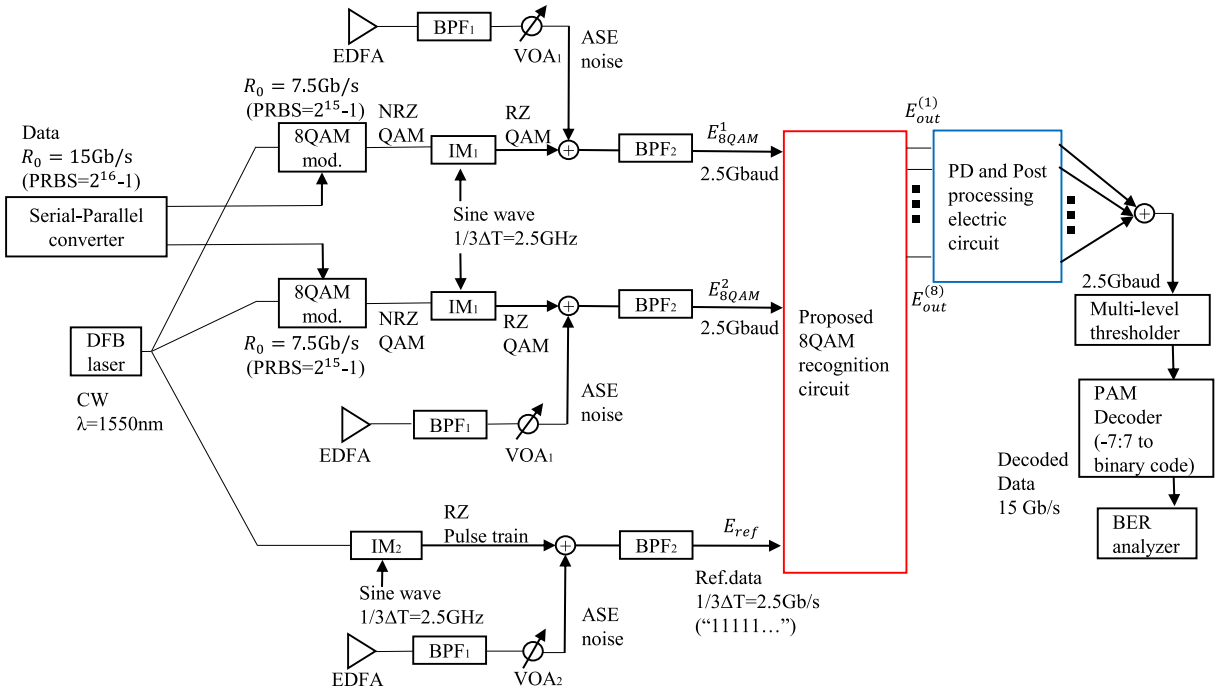

Figure 6.7: Simulation model to evaluate noise tolerance for 2-symbol length minimum output 8QAM recognition circuit

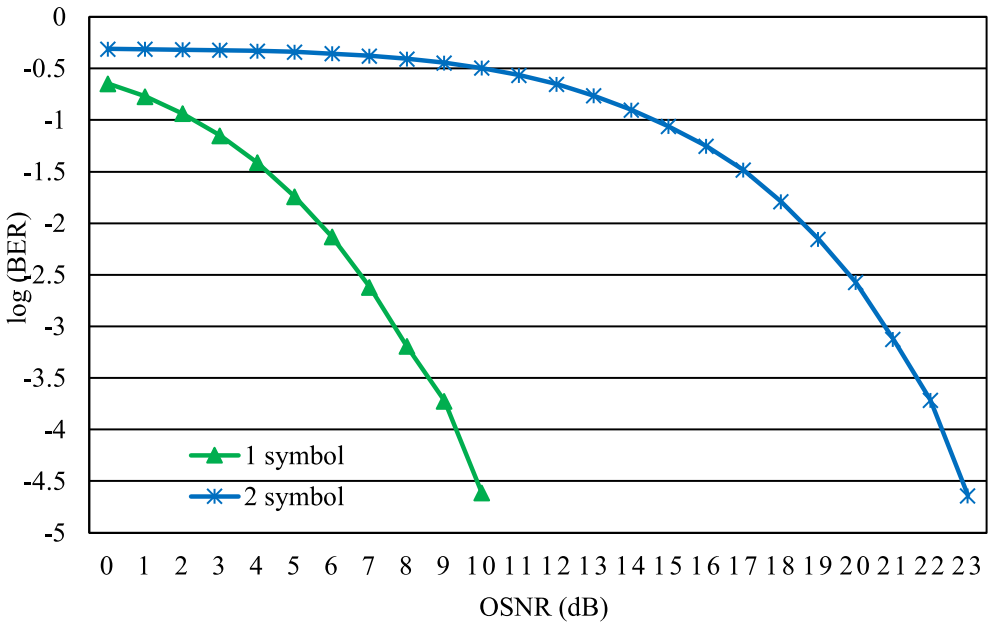

Figure 6.8: Comparison of 1- and 2-symbol BER performance at 2.5 Gbaud symbol rate

Chapter 7

Conclusion

In this thesis work, an existing problem related with electrical signal processing in network nodes has been stated. To meet the expectations of the upcoming traffic growth in communication network, optical signal processing and routing is expected.

Our work is focused on the label recognition function of photonic router and performing it in optical domain. We have reported our proposal on label recognition method of photonic router with waveguide-type circuit for optical 8QAM coded label on the basis of former QPSK code recognition circuit.

With our main proposed circuit, unique null intensities are found for each of the input code combination directly as a theoretical calculation. To verify it, FD-BPM simulation is performed and its results match well with the theoretical calculation. For the identification by non-null or maximum outputs, we added thresholding devices and post processing logical circuit to our main recognition circuit with successful identification of each input code values. To increase the recognizable label numbers, extended 2-symbol length recognition circuit was proposed. As a theoretical calculation, there were null intensities found as well. The maximum intensity value was $0.458E_0^2$ and the second minimum intensity value was $0.001E_0^2$ for scaled circuit. Therefore, a required dynamic range for post processing was around 28 dB.

In communication network, noise tolerance is an important characteristic. Thus, noise tolerance for our proposed circuits was run by Optisystem software. simulation which run for B2B, 2.5-, 5- and 10-Gbaud symbol rate cases. For one symbol minimum recognition circuit, the OSNR values to achieve BER less than 1.0×10^{-3} were 7.8 dB, 10.8 dB and 13.9 dB at 2.5-, 5- and 10-Gbaud symbol rates, respectively. Whereas, for the one symbol maximum recognition circuit, it was found to be 11.6 dB, 14.6 dB and 17.7 dB which was around 4 dB higher than the minimum recognition scheme. As follows, it is realized that minimum recognition circuit is optimal for 8QAM label. A simulation for scaled two symbol minimum recognition circuit was run at 2.5-Gbaud symbol rate and OSNR value at BER less than 1.0×10^{-3} was found as 20.8 dB which is 13 dB higher than one symbol minimum recognition circuit.

In our future work, we will consider to scale the recognition circuit for 3- or more symbol length 8QAM coded labels since the required number of labels in broadband network is enormous. Thereafter, an experimental verification for proposed recognition circuit will be considered as well.

References

[1] A. E. Willner, S. Khaleghi, M. R. Chitgarha, and O. F. Yilmaz, "All-Optical Signal Processing," J. Lightw. Technol., vol. 32, no. 4, pp. 660-680 (2014).

[2] D. J. Blumenthal, B. E. Olsson, G. Rossi, et al., "All-Optical Label Swapping Networks and Technologies," J. Lightw. Technol., vol. 18, no. 12, pp. 2058-2075 (2000).

[3] P. J. Winzer "High-Spectral-Efficiency Optical Modulation Formats," J. Lightw. Technol., vol. 30, no. 24, pp. 3824-3832 (2012).

[4] M. Aljada and K. Alameh, "Passive and Active Optical Bit-pattern recognition structures for multiwavelength optical packet switching networks," Opt. Exp., vol. 15, no. 11, pp. 6914-6925, (2007).

[5] H. Furukawa, T. Konishi, K. Itoh, N. Wada, and T. Miyazaki, "Discrimination of All Types of 4-bit Optical Code by Optical Time-Gating and Designed Label Recognition Filter in Label Recognition Using Optical Correlation," IEICE Trans. Commun., vol. E88-B, no. 10, pp. 3841-3847 (2005).

[6] N. Kawakami, K. Shimizu, N. Wada, F. Kubota, and K. Kodate, "All-Optical Holographic Label Processing for Photonic Packet Switching," Opt. Rev., vol. 11, no. 2, pp. 126-131, (2004).

[7] H. Tsunematsu, T. Arima, N. Goto, and S. Yanagiya,, "Photonic Label Recognition by Time-Space Conversation and Two-Dimensional Spatial Filtering with Delay Compensation," J.Lightw. Technol., vol. 27, no. 4, pp. 2698-2706, (2009).

[8] F. Moritsuka, N. Wada, T. Sakamoto, T. Kawanishi, Y. Komai, S. Anzai, M. Isutsu, and K. Kodate, "Multiple Optical Code-Label Processing Using Multi-Wavelength Frequency Comb Generator and Multi-Port Optical Spectrum Synthesizer," Opt. Exp., vol. 15, no. 12, pp. 7515-7521, (2007).

[9] G. Manzacca, M. S. Moreolo, and G. Cincotti, "Performance Analysis of Multidimensional Codes Generated/Processed by a Single Planar Devices," J. Lightw. Technol., vol. 25, no. 6, pp. 1629-1637, (2007).

[10] H. Hiura, N. Goto, and S. Yanagiya, "Wavelength-Insensitive Integrated-Optic Circuit Consisting of Asymmetric X-junction Couplers for Recognition of BPSK Labels," J. Lightw. Technol., vol. 27, no. 24, pp. 5543-5551, (2009).

[11] Y. Makimoto, H. Hiura, N. Goto, and S. Yanagiya, "Waveguide-Type Optical Circuit for Recognition of Optical QPSK Coded Labels in Photonic Router," J. Lightw. Technol., vol. 27, no. 1, (2009).

[12] K. Inoshita, H. Kishikawa, Y. Makimoto, N. Goto, and S. Yanagiya, "Proposal of Optical Waveguide Circuits for Recognition of Optical QAM Codes," J. Lightw. Technol., vol. 31, no. 13, (2013).

[13] 左貝潤一,“ 導波光学 ”、共立出版, (2004).

[14] 藪徹郎,“ 光導波路解析入門 ”、森北出版, (2007).

[15] Katsunari Okamoto, "Fundamentals of Optical Waveguides," (2006).

[16] 河野健治・鬼頭勤,“ 光導波路解析の基礎 ”、現代工学社、(2003).

[17] Shiva Kumar, and M. Jamal Deen, "Fiber Optic Communications" (2014).

[18] T. Surenkhorol, H. Kishikawa, and N. Goto, "Waveguide-type Optical Circuits for Recognition of Optical 8QAM-coded label," Opt. Eng., vol. 56, no. 10, 107101, (2017).

[19] K. Kitayama, N. Wada,and H. Sotobayashi, "Architectural considerations for photonic IP router based upon code correlation," J. Lightw. Technol., vol.18, no.12, pp.1834-1844, (2000).

[20] K. Inoshita, H. Kishikawa, and N. Goto, "Noise Tolerance in Optical Waveguide Circuits for Recognition of Optical 16 Quadrature Amplitude Codes," Opt. Eng., vol. 55, no. 12, 126105, (2016).

List of achievements

Publication

1. Tumendemberel Surenkhorol, Hiroki Kishikawa, Nobuo Goto, and Khishigjargal Gonchigsumlaa "Waveguide-type Optical Circuits for Recognition of Optical 8QAM-coded label," Optical Engineering, volume 56, number 10, 107101, (2017).

International conferences

1. Tumendemberel Surenkhorol, Hiroki Kishikawa, and Nobuo Goto, "Integrated Optic Circuit for Optical 8QAM Coded Label Recognition in Photonic Router," OSA Advanced Photonics Congress, New Orleans, Louisiana, USA, 24-27 July, 2017.

2. Tumendemberel Surenkhorol, Hiroki Kishikawa, and Nobuo Goto, "Noise Tolerance in Optical Waveguide Circuits for Recognition of Optical 8QAM Codes," Opto-Electronics and Communications Conference (OECC) 2017, Singapore, July 31st- August 4th, 2017.

3. Tumendemberel Surenkhorol, Hiroki Kishikawa, and Nobuo Goto, "Noise Tolerance for Optical Waveguide Circuits for Recognition of 2-symbol Optical 8QAM Codes," Asia Communications and Photonics Conference (ACP) 2017, Guangzhou, China, 10-13 November, 2017.

4. Tumendemberel Surenkhorol, Hiroki Kishikawa, and Nobuo Goto, "Noise-Tolerance Evaluation for Optical 8QAM Coded Label Recognition Circuit," OSA 2019 Advanced Photonics Congress (APC2019), San Francisco, No.SpM3E.2, Jul. 2019.

Domestic conference

1. Tumendemberel Surenkhorol, Hiroki Kishikawa, and Nobuo Goto, "Recognition of Optical 8QAM Coded Labels in Photonic Router," 平成 28 年度電気関係学会四国支連合大会, Tokushima, Japan, 17 September, 2016.